that mammalian epididymal sperm always form E-cadherin/β-catenin complex.

Generation of *β-catenin*-, *α-catenin*- and *E-cadherin*-deficient oocytes. To determine which genes are involved in sperm-oocyte adhesion among *β-catenin*, *α-catenin* and *E-cadherin* genes, three strains (*E-cadherin*$^{floxed/floxed\ 17}$, *β-catenin*$^{floxed/floxed\ 18}$, and *α-catenin*$^{floxed/floxed\ 19}$) with *loxP*-flanked genes were inter-crossed with the transgenic mouse strain (*Tg*$^{ZP3\text{-}cre/+}$) expressing cre-recombinase in an oocyte-specific manner. Offspring (F2) lacking each type of gene (*E-cadherin*$^{floxed/floxed}$*Tg*$^{ZP3\text{-}cre/+}$, *β-catenin*$^{floxed/floxed}$*Tg*$^{ZP3\text{-}cre/+}$ and *α-catenin*$^{floxed/floxed}$*Tg*$^{ZP3\text{-}cre/+}$) were successfully obtained according to the Menderian inheritance rule (see Methods; Supplementary Fig. S3a), and were all viable and normal in size without displaying any overt physical or behavioral abnormalities. When the number of ovulated oocytes from these superovulated offspring was counted and compared with that of oocytes from the control floxed mice, there were no clear differences in the number of ovulated oocytes between the two groups: 11.7 ± 1.4 (n = 25) for *E-cadherin*$^{floxed/floxed}$*Tg*$^{ZP3\text{-}cre/+}$and 13.7 ± 1.9 (n = 22) for *E-cadherin*$^{floxed/floxed}$; 23.2 ± 1.5 (n = 21) for *β-catenin*$^{floxed/floxed}$*Tg*$^{ZP3\text{-}cre/+}$ and 23.2 ± 1.5 (n = 19) for *β-catenin*$^{floxed/floxed}$; 15.6 ± 2.4 (n = 9) for *α-catenin*$^{floxed/floxed}$*Tg*$^{ZP3\text{-}cre/+}$ and 12.4 ± 2.3 (n = 9) for *α-catenin*$^{floxed/floxed}$. Oocytes isolated from each line carrying the *cre-recombinase* gene were not morphologically distinguishable from those from each control floxed line (Supplementary Fig. S3b). To confirm whether oocytes from these gene-disrupted mice exhibit loss of target protein expression, oocytes were subjected to immunocytochemical staining together with oocytes from control floxed mice. E-cadherin, β-catenin and α-catenin were indeed absent from oocytes of *E-cadherin*$^{floxed/floxed}$*Tg*$^{ZP3\text{-}cre/+}$, *β-catenin*$^{floxed/floxed}$*Tg*$^{ZP3\text{-}cre/+}$ and *α-catenin*$^{floxed/floxed}$*Tg*$^{ZP3\text{-}cre/+}$, respectively (Supplementary Fig. S3b). These results suggest that these three genes are not essential for the maturation and ovulation of mouse oocytes.

In epithelial cells, β-catenin is required for localization of E-cadherin on the cell surface, and endocytosis of E-cadherin into the cytoplasm occurs in the absence of β-catenin[20]. In addition, a model was proposed: α-catenin participates to bind to the E-cadherin/β-catenin complex to connect with actin microfilaments under certain specific conditions[9]. In analogy to this, it is possible that cellular localization of E-cadherin, β-catenin and α-catenin is mutually regulated in oocytes. Such a possibility is already depicted in Fig. 1a, in which E-cadherin was co-localized with β-catenin, but not with α-catenin on a wild-type oocyte. To examine whether the formation of E-cadherin/β-catenin complex (possibly E-cadherin/β-catenin/α-catenin complex) is impaired when either one of these composite proteins is deficient, oocytes collected from all of the gene-ablated strains were immunocytochemically assessed for localization of these three proteins (Supplementary Fig. S4a–c). Expression of E-cadherin was strongly reduced on the cell membrane of *β-catenin*-deficient oocytes, but not *α-catenin*-deficient oocytes (Supplementary Fig. S4a *vs.* Fig. S4b). On the other hand, loss of E-cadherin did not affect the localization pattern of β-catenin and α-catenin (Supplementary Fig. S4c). Similar results were also obtained when *α-catenin*-deficient oocytes were examined (Supplementary Fig. S4a). These results indicate that β-catenin regulates the membrane localization of E-cadherin in mouse oocytes.

Sperm-oocyte adhesion or fusion assay. Membrane interaction between oocytes and sperm occurs after the penetration of sperm into ZP (Supplementary Fig. S1a). To monitor such interaction directly, 'ZP-free' *β-catenin*-deficient oocytes after enzymatic digestion of ZP were inseminated with wild-type epididymal sperm (Fig. 3a, b for adhesion assay; Fig. 3c–e for fusion assay). 'ZP-free' oocytes from *β-catenin*$^{floxed/floxed}$ mice were used as a control. When the oocytes were inspected 1 h after insemination and stained with 4',6-diamidino-2-phenylindole (DAPI) after fixation, as depicted in Fig. 3a, the number of sperm adhered to 'ZP-free' *β-catenin*-deficient oocytes was significantly reduced (Fig. 3b) compared to sperm bound to control oocytes. Similarly, when DAPI-preloaded oocytes were inspected 1 h after insemination, as depicted in Fig. 3c, the relative rate of 'ZP-free' *β-catenin*-deficient oocytes fused with sperm was also significantly reduced (39.2 ± 12.7 *vs.* 100.0 for control oocytes; $P<0.003$; Fig. 3d, e). We next examined the expression pattern of CD9, an essential protein for fusion[4], in *β-catenin*-deficient oocytes immunocytochemically and immunobiochemically to assess the ability of wild-type C57BL/6N sperm to fuse with their membrane. CD9 was expressed on the plasma membrane of 'ZP-free' *β-catenin*-deficient oocytes at a level comparable to that of 'ZP-free' control oocytes (Supplementary Fig. S5a). The total amount of CD9 quantified by immunoblotting in *β-catenin*-deficient oocytes was comparable to that of control oocytes (Supplementary Fig. S5b). These findings suggest that β-catenin is involved in sperm-oocyte adhesion.

***In vitro* fertilizing ability of *β-catenin*-deficient oocytes.** To know how fertilization is influenced by the dysfunction of sperm-oocyte adhesion, we determined the fertilization rate of *β-catenin*-deficient oocytes. The *β-catenin*-deficient oocytes surrounded by cumulus cells (herein referred to as 'cumulus-intact' oocytes) were isolated from oviducts and directly subjected to IVF with wild-type sperm, as depicted in Fig. 3f. 'Cumulus-intact' oocytes from *β-catenin*$^{floxed/floxed}$ mice were used as a control. When the oocytes were inspected 24 h after insemination, the relative rate of *β-catenin*-deficient oocytes fused with sperm was not reduced (Fig. 3g). Quantitative analysis revealed that the rate of *β-catenin*-deficient oocytes fused with sperm was rather enhanced (119.6 ± 4.6 *vs.* 100.0 for control oocytes; $P<0.02$; Fig. 3h), in contrast with the results of the previous adhesion/fusion assay (Fig. 3a–e). This is probably due to the occasional presence of the oocytes fused to sperm, which failed to develop to the two-cell stage; however, the fact that certain embryos developed to the two-cell stage would not exclude the possibility of pathogenetic activation of oocytes. On the other hand, the IVF rate (which is evaluated by the development of fertilized oocytes to the two-cell stage) was comparable between the two groups (Fig. 3i).

We further confirmed the above point by counting litters obtained through mating between *β-catenin*$^{floxed/floxed}$*Tg*$^{ZP3\text{-}cre/+}$ females and *β-catenin*$^{floxed/floxed}$ males. The control *β-catenin*$^{floxed/floxed}$ females were similarly mated. The litter size of *β-catenin*$^{floxed/floxed}$*Tg*$^{ZP3\text{-}cre/+}$ females was 5.3 ± 0.4, which was comparable with that of control females (5.8 ± 0.4) (Supplementary Fig. S6). These results indicate that oocytes lacking β-catenin expression reduce the ability to adhere with sperm, but sustain the ability to fuse with sperm as well as the total reproductive ability needed for delivering pups.

Possible involvement of β-catenin in transition of membrane adhesion to fusion. To examine the dynamics of β-catenin at sperm-oocyte membrane adhesion, alteration in the localization pattern of β-catenin at the sperm attachment sites of the *in vitro* fertilized "zona-free" oocyte was monitored (Fig. 4a–c). Before sperm attachment, β-catenin-rich patches (as shown in Fig. 1b) were clearly detected on the surface of an oocyte (upper left panel of Fig. 4a); however, these patches became undetectable 30 min after sperm attachment (arrows in the lower left panel; Fig. 4a). Furthermore, β-catenin was abundantly present in the capacitated sperm head (upper middle and right panels of Fig. 4a) before sperm attachment, but the amount of β-catenin in sperm heads was also greatly reduced after insemination (arrows in the lower middle and right panels; Fig. 4a). In addition, β-catenin was localized in the sperm head, although its localization pattern was slightly different in each sperm. Notably, β-catenin tended to be concentrated at ES (Fig. 2c; Supplementary Fig. S2; Fig. 4a).

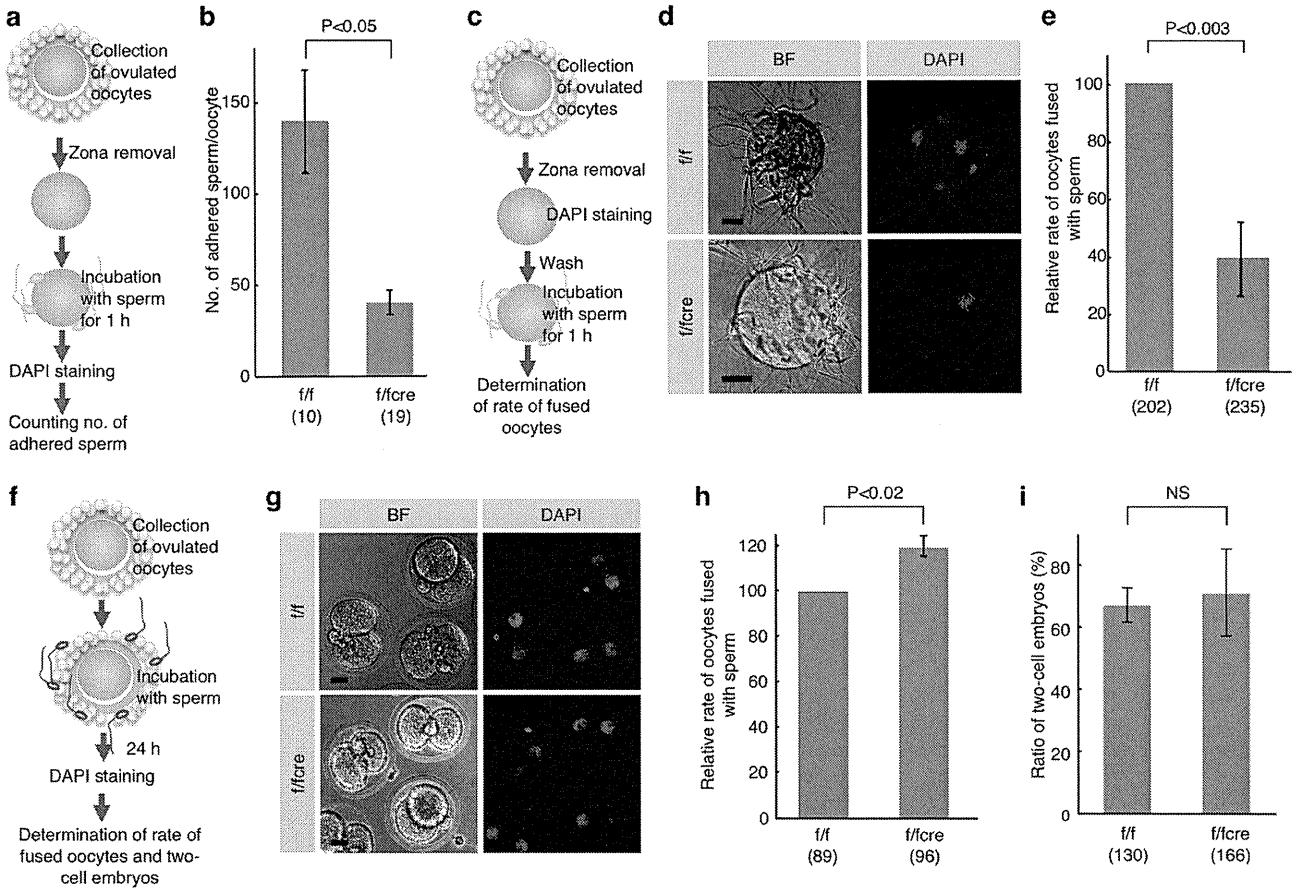

Figure 3 | *In vitro* fertilizing ability of *β-catenin*-deficient oocytes. (a) Experimental flow for testing sperm-oocyte membrane 'adhesion', and comparison of the number of wild-type sperm adhered to an 'zona-free' oocyte between f/fcre and f/f oocytes. After ZP removal, 'zona-free' oocytes were mixed with sperm for 1 h. (b) The number of sperm adhered to an oocyte was counted by DAPI-derived fluorescence in sperm heads on the surface of an oocyte. Parentheses indicate the number of oocytes examined. Values are the mean ± standard error (SE). (c) Experimental flow for testing sperm-oocyte membrane 'fusion' and fused sperm (shown as DAPI-positive sperm) in 'zona-free' *β-catenin*-deficient (f/fcre) and control (f/f) oocytes. After ZP removal, subsequent preincubation for 20 min in the presence of DAPI and washing, 'zona-free' oocytes were mixed with the wild-type sperm for 1 h. (d) Comparison of oocytes fused with sperm between f/fcre and f/f oocytes. BF, bright field. Bars: 20 μm. (e) Comparison of the relative rate of oocytes fused with sperm between f/fcre and f/f oocytes. Only oocytes having at least one fused sperm were counted. The comparative values relative to the control (f/f oocytes; set to 100.0) were displayed as the relative rate of fused oocytes. Parentheses indicate the number of oocytes examined in triplicate experiments. Values are the mean ± SE. (f) Experimental flow for testing sperm-oocyte membrane interaction and fused sperm in two-cell embryos developing from 'cumulus-intact' *β-catenin*-deficient (f/fcre) and control (f/f) oocytes. DAPI staining was performed to detect fused sperm on the developing two-cell embryos. (g) Comparison of oocytes fused with sperm between "cumulus-intact" f/fcre and f/f oocytes. Bars: 20 μm. (h) Comparison of the relative rate of oocytes fused with sperm between "cumulus-intact" f/fcre and f/f oocytes. Parentheses indicate the number of oocytes examined in triplicate experiments. Values are the mean ± SE. (i) Comparison of the ratio of oocytes developing to two-cell stage 24 h after fertilization between "cumulus-intact" f/fcre and f/f oocytes, according to the procedure described in (f). Parentheses indicate the total number of oocytes examined in triplicate experiments. NS, not significant. Values are the mean ± SE.

These findings could also be supported by measurement of fluorescent intensities of β-catenin (Fig. 4b, c). When fluorescence intensity at the equator of an oocyte (dotted line in the upper image of the left panels; Fig. 4a) was compared with that in the region of an oocyte adhered to sperm (dotted line in the lower image of the left panels; Fig. 4a), intense localization of β-catenin in the oocyte exhibiting no sperm attachment was observed beneath the oocyte membrane (arrows in the upper graph; Fig. 4b); however, 30 min after sperm attachment, the fluorescent intensity of β-catenin beneath the oocyte membrane was markedly reduced (arrows in the lower graph; Fig. 4b). Concomitantly, fluorescence intensity throughout the entire sperm (dotted lines in the right panels; Fig. 4a) was quantitatively compared before and after sperm adhesion to the oocyte membrane (Fig. 4c). Before attachment to the oocyte membrane, β-catenin was broadly localized in the sperm head (corresponding to the DAPI-stained region), mid-piece and part of the tail (Fig. 2c, d; upper graph of Fig. 4c); however, after attachment to the oocyte membrane, the intensity of β-catenin in the sperm head (but not in a mid-piece and tail) was markedly decreased (arrows in the lower middle and right panels of Fig. 4a; lower graph of Fig. 4c). Moreover, to confirm that the amount of β-catenin is reduced at steps between sperm-oocyte adhesion and fusion, localization pattern of β-catenin at the sperm attachment sites of the *in vitro* fertilized "zona-free" *CD9*-deficient oocyte was monitored (Fig. 4d, e). Before sperm attachment, intense localization of β-catenin (as shown in the upper left panel of Fig. 4a) was clearly seen on the surface of an oocyte (upper middle panel of Fig. 4d); however, these patches became undetectable 30 min after sperm attachment (arrows in the lower middle panel; Fig. 4d). These findings were also confirmed by measurement of fluorescent intensities of β-catenin (Fig. 4e). When

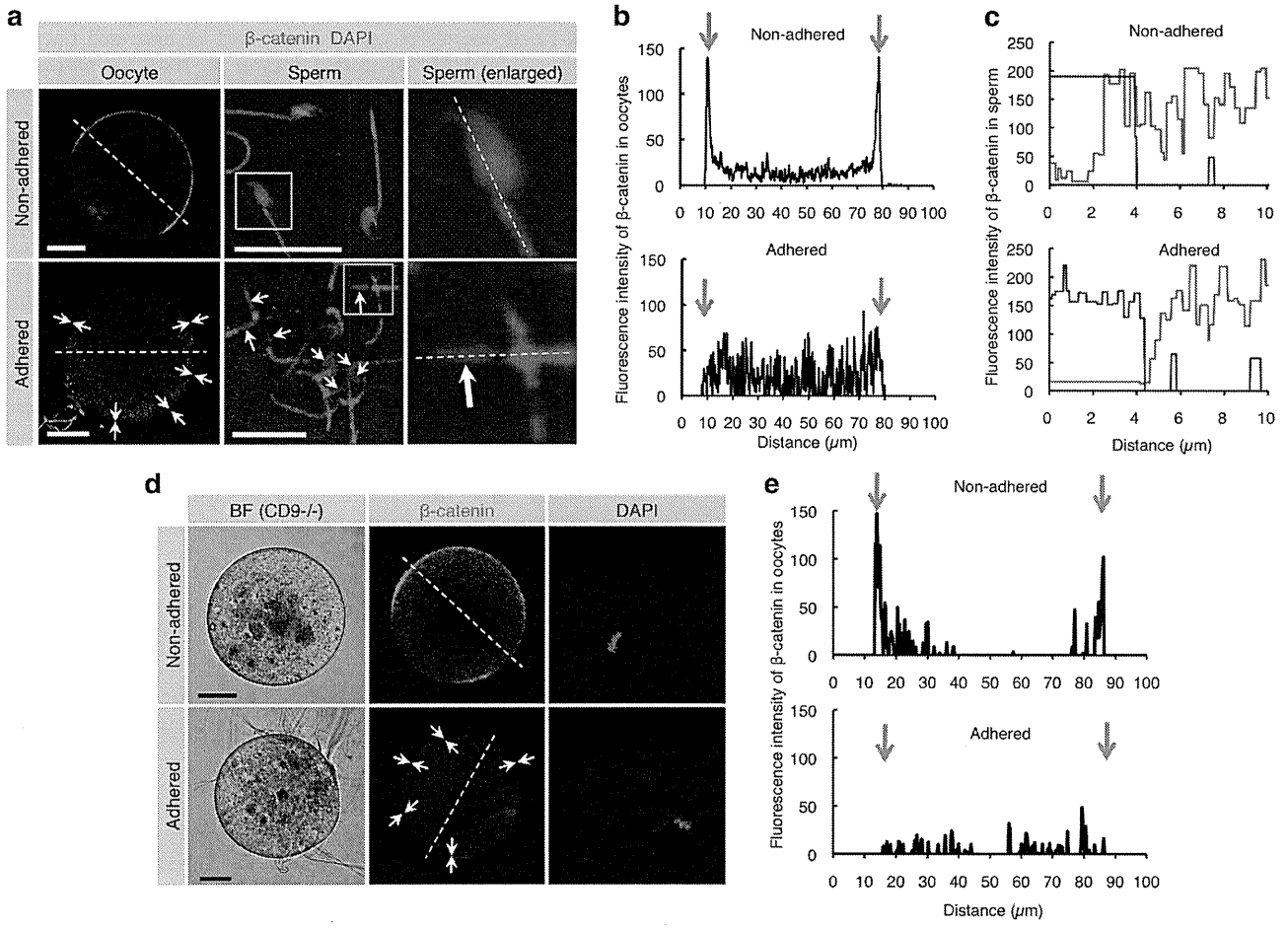

Figure 4 | Reduced levels of β-catenin localized beneath the cell membrane of both oocytes and sperm after membrane adhesion. (a) β-catenin disassembly induced by membrane adhesion in oocytes and sperm. In the 'Non-adhered' group (upper panels), ZP-denuded C57BL/6N oocytes were stained with DAPI and subsequently reacted with anti-β-catenin mAb. Also, epididymal sperm were stained with DAPI and anti-β-catenin mAb. In the 'Adhered' group (lower panels), ZP-denuded C57BL/6N oocytes were stained with DAPI and then subjected to IVF for 30 min prior to incubation with anti-β-catenin mAb. Arrows indicate areas where fluorescent intensities of β-catenin are reduced. In each panel, boxes in middle sets of panels were enlarged and shown on the right. Scale bars: 20 and 10 μm in left and middle panels, respectively. (b) Fluorescence intensities of oocytes before and after sperm-oocyte adhesion. Fluorescence intensities were measured after being traced along dotted lines in the left panels of (a). Arrows indicate both sides of the oocyte cell membranes. (c) Fluorescence intensities of sperm before and after sperm-oocyte adhesion. Fluorescence intensities were measured after being traced along dotted lines in the right panels of a. Red and blue lines indicate fluorescent intensities for β-catenin and DAPI, respectively. (d) β-Catenin disassembly induced by membrane adhesion in oocytes and sperm. In the 'Non-adhered' group (upper panels), ZP-denuded *CD9-/-* oocytes were stained with DAPI and subsequently reacted with anti-β-catenin mAb. In the 'Adhered' group (lower panels), ZP-denuded *CD9-/-* oocytes were preloaded with DAPI as depicted in Fig. 3c and then subjected to IVF for 30 min prior to incubation with anti-β-catenin mAb. Arrows indicate areas where fluorescent intensities of β-catenin are reduced. In each panel, Scale bars: 20 μm. (e) Fluorescence intensities of *CD9-/-* oocytes before and after sperm-oocyte adhesion. Fluorescence intensities were measured after being traced along dotted lines in the left panels of d. Arrows indicate both sides of the oocyte cell membranes.

fluorescence intensity at the equator of an oocyte (dotted line in the upper image of the middle panel; Fig. 4d) was compared with that in the region of an oocyte adhered to sperm (dotted line in the lower image of the middle panel; Fig. 4d), intense localization of β-catenin in the oocyte exhibiting no sperm attachment was observed beneath the oocyte membrane (arrows in the upper graph; Fig. 4e); however, 30 min after sperm attachment, the fluorescent intensity of β-catenin beneath the oocyte membrane was markedly reduced (arrows in the lower graph; Fig. 4e). These collective data imply that alteration in the localization of β-catenin in both sperm and oocyte membranes may contribute to the transition of cell adhesion to fusion.

Generally, in the absence of Wnt signal, E-cadherin-free cytoplasmic β-catenin is rapidly degraded due to "ubiquitination", while only membrane-anchored β-catenin, which is associated with E-cadherin, is resistant to such degradation[21]. Since the fluorescence intensity of β-catenin beneath cell membranes was greatly reduced in both sperm and oocytes after membrane adhesion, ubiquitination may be involved in such reduction. In other words, degradation of β-catenin may be involved in the transition from adhesion to fusion upon sperm-oocyte interaction. To test this possibility, we employed an inhibitor of the ubiquitination pathway to investigate whether it can disturb sperm-oocyte fusion. UBE1-41, a specific inhibitor of ubiquitin-activating enzyme 1 (UBE1), is known to impair antigen-induced FcεRI ubiquitination and internalization[22] and to inhibit melanocortin-4 receptor internalization via ubiquitination[23]. To determine the optimal concentration of UBE1-41, we first assessed sperm-oocyte interaction by co-incubation of sperm and

oocytes in TYH medium containing various amounts of UBE1-41 (0, 1, 5, 10, 20 or 50 μM). We finally decided to use 10 μM UBE1-41, because treatment with more than 20 μM UBE1-41 caused deleterious effects on oocytes. Notably, this concentration (10 μM) appears to be lower than that (50 μM) reported previously[22]. "Zona-free" oocytes treated with 10 μM UBE1-41 for 30 min were incubated with sperm and the ratio of fused oocytes was measured (Fig. 5a). As depicted in Fig. 4a, c, the fluorescence intensity of β-catenin beneath cell membranes was greatly reduced in the untreated oocyte after membrane adhesion with sperm (arrows in the upper left panel; Fig. 5b); however, intense localization of β-catenin was observed beneath the oocyte membrane in the oocyte treated with UBE1-41 even after membrane adhesion with sperm (arrows in the lower left panel; Fig. 5b), and β-catenin-rich patches (oocyte before membrane adhesion; Fig. 1b) were clearly detected on the surface of the oocyte (lower right panel; Fig. 5b). The rate of oocyte fusion with sperm was inversely correlated with the intense localization of β-catenin beneath the cell membrane: treatment with UBE1-41 lowered the rate of fused oocytes in contrast with that of untreated oocytes (51.7 ± 6.2 for UBE1-41-treated oocytes *vs.* 100.0 for untreated oocytes; $P<0.0001$; Fig. 5c; Supplementary Fig. S7). This result suggests that β-catenin ubiquitination leading to degradation is involved in transition from membrane adhesion to fusion. Given this background, it seems likely that the loss of β-catenin facilitates sperm-oocyte fusion. In other words, the fusing ability of *β-catenin*-deficient oocytes should be unaffected by treatment with UBE1-41. In fact, *β-catenin*-deficient oocytes exhibited fusing ability, although they were unable to adhere to sperm (Fig. 3). Furthermore, treatment of $\beta\text{-catenin}^{floxed/floxed}Tg^{ZP3\text{-}cre/+}$ oocytes with UBE1-41 did not affect the rate of fused oocytes (90.6 ± 11.3 for UBE1-4-treated oocytes *vs.* 100.0 for untreated oocytes; Fig. 5d). By contrast, similar treatment of $\beta\text{-catenin}^{floxed/floxed}$ oocytes resulted in reduction of their fusing ability, as expected (55.3 ± 11.5 for UBE1-4-treated oocytes *vs.* 100.0 for untreated oocytes; $P<0.02$; Fig. 5d). These results led us

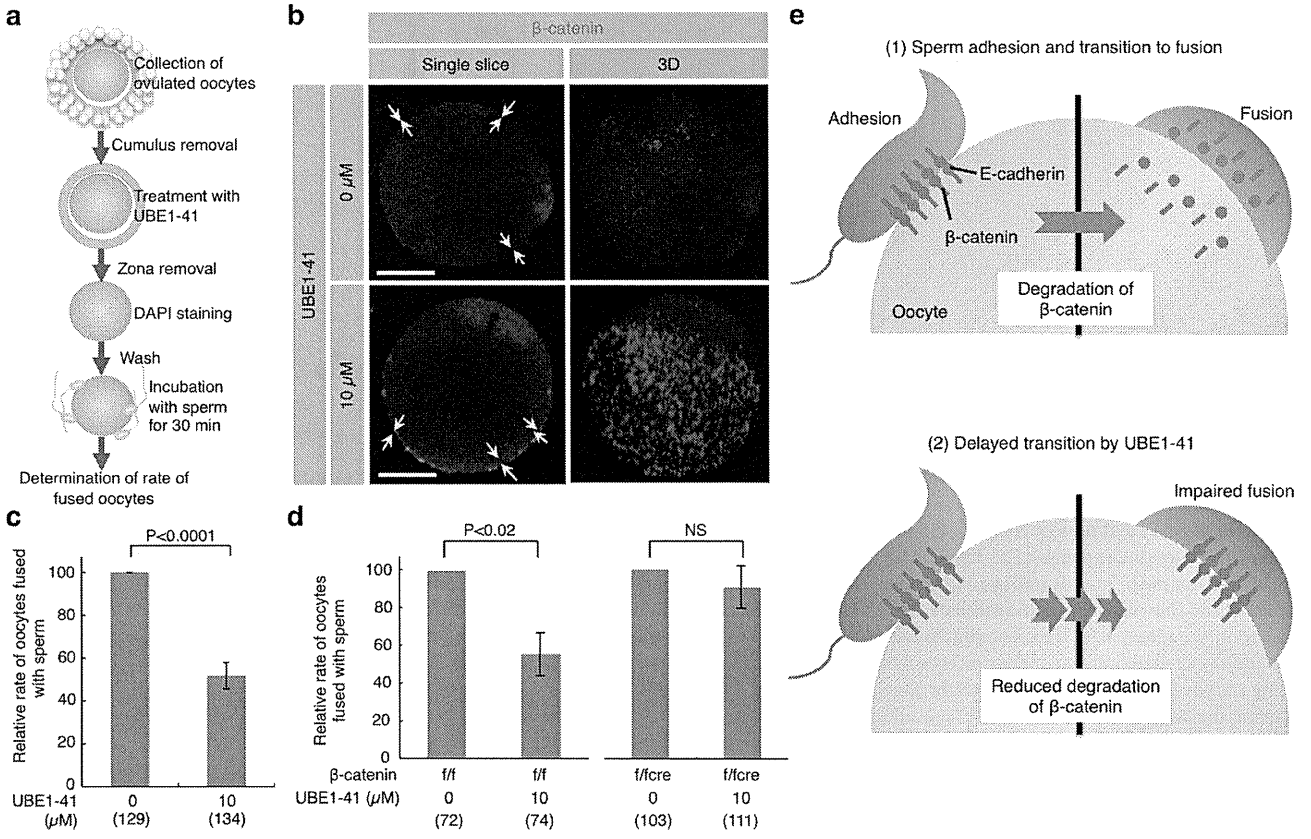

Figure 5 | Reduced fusing ability of oocytes treated with UBE1-41, an inhibitor of ubiquitination. (a) Experimental flow. Cumulus cells attached to the oocytes collected from oviducts were removed. The oocytes were then treated with UBE1-41 for 30 min, followed by ZP removal. After 20-min incubation with DAPI-containing medium and subsequent washing, 'zona-free' oocytes were mixed with the sperm and incubated for 30 min. Only oocytes having at least one fused sperm were counted as fused oocytes. (b) Sustained expression of β-catenin on the surface of "zona-free" wild-type oocytes treated with UBE1-41 after membrane adhesion with sperm. Arrows indicate oocyte cell membranes where β-catenin deposition is noted. One sperm fused with the untreated oocyte (upper panel), but not with the UBE1-41-treated oocyte (lower panel). To focus on the β-catenin expression, only fluorescent images are shown. Single slice, Image captured when the diameter of an oocyte was longest; 3D, 3-dimensional image reconstructed from serial scanned images. Bars: 20 μm. (c) Decreased number of fused sperm on "zona-free" wild-type oocytes after treatment with UBE1-41. The relative rate of oocytes carrying fused sperm was compared between UBE1-41-treated and -untreated wild-type oocytes. The comparative values relative to the control (set to 100.0) are displayed as the relative rate of fused oocytes. As described in the legend of Fig. 3c, oocytes fused with sperm are defined as those with at least one DAPI-positive sperm. (d) Comparison of the relative rate of oocytes carrying fused sperm between UBE1-41-treated and untreated oocytes (*β-catenin*-deficient (f/fcre) *vs. β-catenin*-intact (f/f) oocytes). Comparison was made as described in (c). NS, not significant. Parentheses indicate the total number of oocytes examined in triplicate experiments. Values are the mean ± SE. (e) A model of the possible role of β-catenin in transition from membrane adhesion to fusion. At fertilization (as described in (1)), adhesion of sperm to the surface of an oocyte is mediated by E-cadherin/β-catenin complex; however, subsequent fusion requires rapid degradation of β-catenin. On the other hand, in the presence of UBE1-41 (as described in (2)), adhesion occurs normally, but fusion is impaired since UBE1-41 inhibits degradation of β-catenin.

to consider that β-catenin may be accumulated around sperm attachment sites through the formation of a protein complex with E-cadherin, but immediately diminished when sperm-oocyte fusion occurred. This transient formation of such complex encouraged us to suppose that the E-cadherin/β-catenin complex plays an important role in the transition from membrane adhesion to membrane fusion during sperm-oocyte interaction (Fig. 5e).

Discussion

Membrane fusion occurs after membrane adhesion. Such a process is also true for sperm-oocyte interaction[1]. Our present results indicate that both E-cadherin and β-catenin are involved in sperm-oocyte membrane adhesion. This is demonstrated by the fact that *β-catenin*-deficient oocytes can fuse to sperm, and develop normally to term.

E-cadherin is involved in homophilic adhesion between epithelial cells, and transduces external signaling via α-catenin and β-catenin[9]. In contrast, E-cadherin remains essential for basic cell-cell adhesion, even in the absence of α-catenin, in human prostate carcinoma PC3 cells[24], suggesting that the formation of E-cadherin/β-catenin/actin microfilament complex is proceeded by other molecule(s) in the absence of α-catenin. In analogy, at sperm-oocyte adhesion, association between the E-cadherin/β-catenin complex and actin microfilaments may be mediated by molecule(s) other than α-catenin or the E-cadherin/β-catenin complex itself can directly bind to actin microfilaments, although evidence for this remains to be provided.

Rapid reduction in the level of β-catenin occurs after increased ubiquitination and degradation through a proteosomal pathway[21]. N-Acetyl-Leu-Leu-Nle-CHO (ALLN), a specific inhibitor of the proteolytic activity of proteasomes is reported to inhibit sperm-oocyte fusion upon fertilization[25], implying that the ubiquitination-proteasome pathway may play a role in sperm-oocyte interaction by regulating the quantity of β-catenin on sperm and oocyte membranes. Giving that β-catenin is present on the sperm head and oocyte surface, and that its elimination impairs sperm-oocyte adhesion (see Fig. 3b), it is conceivable that the ubiquitination-proteasome pathway is a key that mediates phase transition from membrane adhesion to fusion, as genetic studies in *C. elegans* have identified multiple roles for the ubiquitin system in early development[26].

Taken together, our results propose a model regarding the transition from membrane adhesion to fusion upon sperm-oocyte interaction (Fig. 5e). Before sperm-oocyte adhesion, both sperm and oocyte retain the β-catenin/E-cadherin complex, a complex important for sperm-oocyte adhesion. Once sperm-oocyte adhesion occurs, β-catenin is immediately ubiquitinated and probably degraded in both the sperm and oocyte, thereby initiating membrane fusion between these two cells; however, in oocytes treated with UBE1-41, ubiquitination of β-catenin associated with sperm-oocyte adhesion is suppressed, which will cause impaired fusion between sperm and oocyte. This sperm-oocyte adhesion and subsequent fusion appears to be each independent phenomena, since the absence of β-catenin results in a reduction in the ability of sperm to adhere to an oocyte, but sperm-oocyte membrane fusion occurs normally.

Similarly, importance of interchange between stabilization and degradation of β-catenin has been described at several developmental aspects, such as mesenchymal cell proliferation[27] and primordial germ cell development[28]. Forced expression of a mutated β-catenin that is resistant to degradation causes developmental arrest at specific sites and time[27,28]. However, its deficiency has no impact on embryogenesis, probably due to compensation of other molecules that play roles similar to β-catenin[27, 28]. Probably, degradation of β-catenin that occurs at appropriate stage and place is needed for normal development of an embryo/fetus and therefore β-catenin may be an important molecule that mediates as a molecular switch in embryogenesis. Our present results showed that although the cell membrane of *β-catenin*-deficient oocytes exhibit reduced ability to adhere sperm (Fig. 3b), these oocytes could be successfully fertilized, indicating that β-catenin contributes partly to sperm-oocyte membrane adhesion, but does not play an essential role in this event. It will be claimed that ZP removal by acidic Tyrode's solution can change cell surface protein composition or carbohydrate structure, which may affect sperm-oocyte interaction to some extents. Our present data, however, clearly suggest that β-catenin degradation is associated with transition from adhesion to fusion upon interaction between sperm and oocyte.

In human trophoblastic cells, an interrelationship between cell differentiation/ fusion and reduced expression of E-cadherin has been pointed out[29]. When the isolated mononuclear cytotrophoblasts are cultured, they tend to aggregate and then fuse to form syncytia. During this process, E-cadherin is detectable at the cell-cell contact sites of an aggregate. However, the fusing cytotrophoblasts (but not non-fusing cytotrophoblasts) exhibit marked reduction in the level of E-cadherin. Notably, exposure of the non-fusing cells to 8-bromo cyclic AMP causes reduced expression of E-cadherin, and induces their cellular fusion and syncytium formation. These results suggest that down-regulation of E-cadherin gene expression coincides with cell fusion, and evoke us to suppose that remodeling of the adhesion complex on the cell surface would induce subsequent cell fusion. Beside E-cadherin, junctional proteins found in tight and adherens junctions such as integral membrane, adaptor, regulator and signaling proteins are recently thought to be important as epithelial and endothelial barriers[30]. They can reversibly increase paracellular transport and drug delivery with less toxicity, indicating that alteration in lipid composition at cell surface membrane, as exemplified by alteration of cholesterol efflux, results in modulation of cellular junctions. Based on these results, we consider that remodeling or degradation of adhesion complex may change lipid composition in a cell membrane, which will then provide microenvironments where cell fusion occurs.

When the fusion step is genetically defective, sperm never fuses with the partner oocyte, as previously shown by using *CD9*-deficient oocytes and *Izumo1*-deficient sperm[3,5,6]. Furthermore, we showed that the presence or absence of β-catenin in oocytes does not affect the expression and localization of CD9 (see Supplementary Fig. S5). In addition, we also observed that the presence or absence of CD9 does not affect the change of β-catenin localization in oocytes before and after adhesion to sperm (see Fig. 4d, e). A couple of these results suggest that β-catenin is independent from CD9 tetraspanin network. These findings evoked us to suppose that the adhesion step may be distinguishable from the fusion step in mammalian fertilization. Interestingly, Jégou *et al.* (2011) recently demonstrated that CD9 is indeed involved in the sperm-egg binding step. This suggests a possible role of CD9 in sperm-oocyte adhesion, but does not exclude the previous finding that CD9 is involved in fusion[31]. Although further investigation on the role of CD9 molecule in sperm-oocyte adhesion and subsequent fusion is needed, it seems likely at present that CD9 may be involved in maintaining the strength of adhesion force on the oocyte cell membrane. Its absence would cause unstable adhesion force, resulting in decreased fertilizing ability of sperm.

In conclusion, we have shown that 1) β-catenin plays a role in sperm-oocyte membrane adhesion upon fertilization; and 2) β-catenin is also involved in the transition of membrane adhesion to fusion, a phenomenon essential for fertilization, and proteasome-mediated regulation of β-catenin is important in such sperm-oocyte fusion.

Methods

Antibodies. Two mAbs against mouse E-cadherin used for immunostaining and immunoblotting (No. ECCD-2; Takara-Bio) and immunoprecipitation (No. 36; BD). Two mAbs against mouse β-catenin were used for immunoprecipitation (No. C2206; Sigma) and immunostaining (No. 15B8; Sigma). A mAb against β-catenin (No. 14; BD) was used for immunoblotting. A polyclonal antibody against mouse α-catenin

(No. C2081; Sigma), Cy3-conjugated mAb against C-terminal peptide conserved in β- and γ-actin isoforms (No. AC-40; Sigma), and FITC-conjugated mAb against β-tubulin (No. TUB2.1; Sigma) were used. A mAb against N-cadherin was used for immunoblotting (No. 32; BD). ECCD-2, which recognizes an epitope in the extracellular region of E-cadherin, bind to E-cadherin on the cell membrane without permeabilization[32].

Immunostaining. Mouse oocytes were collected from oviducts of 8- to 12-week-old C57BL/6N superovulated mice (Japan SLC Inc.). The oocytes were fixed for 20 min at room temperature in a solution (termed PFA-GLA-PVP) containing 2% paraformaldehyde (PFA), 0.1% glutaraldehyde (GLA) and 0.1% polyvinylpyrolidone (PVP). After washing in phosphate-buffered saline (PBS), they were permeabilized with 1% Triton X-100 in PBS, and washed 3 times in PBS. The oocytes were then incubated with the primary antibodies (Abs) (2.5 μg/ml) in HEPES-buffered saline (HBS) containing 10 mM HEPES (pH 8.0), 0.15 M NaCl and 3% fetal bovine serum (FBS) for 2 h at 4°C. These oocytes were next treated with the secondary Abs (1.25 μg/ml), Alexa488- or Alexa546-conjugated IgG (Molecular Probes), and washed 3 times in HBS. Mouse sperm were also isolated from the cauda epididymides of 8- to 12-week-old C57BL/6N male mice by teasing them in TYH medium[33], and immunostained as described above. In addition, sperm were collected from 24-week-old KAT strain[16] males of the *Suncus murinus*, kindly provided by Dr. Senichi Oda and immunostained as described above. These immunostained sperm were then counterstained with DAPI (WAKO) at the final concentration of 10 μg/ml in HBS for 30 min at 4°C, and washed 3 times by transfer to HBS.

Sectioned fluorescent images were captured by a confocal microscope (LSM 510 model; Carl Zeiss), and transformed into three-dimensional (3D) images by LSM Image Brower Version 4.2.0.121. The fluorescence intensities of target proteins were then measured based on the 3D images (Supplementary Fig. S1d, e; Fig. 1b), and compared between latA-untreated and -treated oocytes (Fig. 1d), unpermeabilized and permeabilized sperm (Fig. 2c, d), and oocytes and sperm before and after membrane adhesion (Fig. 4a–c). All animal experiments were performed according to protocols approved by the Institutional Animal Care and Use Committee at the National Institute for Child Health and Development.

Immunoblotting and immunoprecipitation. The sperm suspension (ca. 3.0×10^6 cells) prepared from C57BL/6N males was collected by centrifugation, as described by Inoue *et al.*[3] A total of 200 oocytes were collected and then lysed in Laemmli's SDS sample buffer, boiled, resolved in SDS-PAGE on an 8% acrylamide gel, and immunoblotted as described previously[34]. Mouse embryonic carcinoma P19 cells[35] were were used as a positive control. For immunoprecipitation, Sakakibara *et al.*[34] describe this procedure in more detail citing references[36]. Proteins from sperm (ca. 3.0×10^6 cells) (Fig. 2b) or 905 oocytes (Fig. 1c) were immunoprecipitated with Abs (2.5 μg/ml) for 6 h at 4°C. The presence of β-tubulin was detected and used as an internal loading control.

Actin disassembly induced by latA treatment. Mouse oocytes collected from oviducts of superovulated mice were incubated in TYH medium containing 10 μM latA (Molecular Probes) for 1 h at 37°C, and fixed in PFA-GLA-PVP solution. After permeabilization with 1% Triton X-100, oocytes were doubly immunostained by mAbs against actin and β-catenin as mentioned in the 'Immunostaining' section. The fluorescence intensities at the equator, as indicated by dotted lines, were then analyzed as described in the 'Immunostaining' section.

Generation of mice with gene-ablated oocytes. To produce oocytes with a single gene deleted, floxed mutant mice for *E-cadherin*[17], *β-catenin*[18] or *α-catenin* gene[19] were cross-mated with transgenic (Tg) mice expressing *cre-recombinase* in an oocyte-specific manner under the control of oocyte-specific ZP protein 3 (ZP3) promoter ($Tg^{ZP3\text{-}cre/+}$), kindly provided by Dr. Barbara B. Knowles[37]. The F1 offspring, so-called $E\text{-}cadherin^{floxed/floxed}Tg^{ZP3\text{-}cre/+}$, $\beta\text{-}catenin^{floxed/floxed}Tg^{ZP3\text{-}cre/+}$ and $\alpha\text{-}catenin^{floxed/floxed}Tg^{ZP3\text{-}cre/+}$, were propagated through brother-sister mating. The presence of the *cre-recombinase* gene in these offspring was detected by PCR analysis using the following set of primers: Cre-S (5'-TGATGAGGTTCGCAAGAACC-3'; nucleotide no. 170 to 189 (GenBank Accession no. AB449974.1)) and Cre-A (5'-CCATGAGTGAACGAACCTGG-3'; nucleotide no. 539 to 558 (GenBank Accession no. AB449974.1)); this primer set yielded a band of 389 bp.

Determination of litter size and *in vitro* fertilization (IVF). To determine the litter size, the number of pups delivered from an 8- to 12-week-old female (offspring of $\beta\text{-}catenin^{floxed/floxed}Tg^{ZP3\text{-}cre/+}$ mice) was recorded after mating for two months by placing an 8- to 12-week-old C57BL/6N male in the cage.

For IVF, oocytes were collected from the oviductal ampulla region of superovulated $\beta\text{-}catenin^{floxed/floxed}Tg^{ZP3\text{-}cre/+}$ females (8 to 12 weeks old) 14 to 16 h after hCG injection, and placed in a 30-μl drop of TYH medium covered with paraffin oil (Nacalai) equilibrated with 5% CO_2 in air at 37°C. Sperm collected from the epididymides of 8- to 12-week-old C57BL/6N males were induced to capacitate by incubating in TYH medium for 90 min in an atmosphere of 5% CO_2 in air at 37°C before insemination. The final concentration of sperm added to the oocytes was 1.5×10^5 sperm/ml. The oocytes collected from *floxed/floxed* mice were also inseminated with C57BL/6N sperm as a control.

To count the number of sperm fused to an oocyte, cumulus cells were dispersed from oocytes by incubating them for 10 min at 37°C in TYH medium containing hyaluronidase (300 μg/ml; Merk4Biosciences), and then the oocytes were denuded of the ZP by brief incubation in acid Tyrode's solution (Sigma). The 'zona-free' oocytes were preincubated with DAPI at the final concentration of 10 μg/ml in TYH medium for 20 min at 37°C, and washed 3 times by being transferred to separate drops of TYH medium. DAPI is a fluorescent dye that can slowly permeate the living cell membrane (semi-permeable) and hardly leaks out of cells after washing, relative to Hoechst33342 (permeable), as shown in Invitrogen's instructions. This preincubation procedure with DAPI enables the staining of only fused sperm nuclei, probably through a mechanism in which the dye present within an oocyte is transferred to fused sperm upon membranous fusion. C57BL/6N sperm (ca. 1.5×10^5 sperm/ml) were added to a 30-μl drop of TYH medium containing 30 DAPI-treated 'zona-free' oocytes and then the dish was incubated for 1 h at 37°C. After incubation, the oocytes were fixed with PFA-GLA-PVP solution for 20 min at room temperature. The rate of oocytes fused with sperm was determined by counting DAPI-transferred sperm on an oocyte under a fluorescence microscope. In this case, oocytes fused with sperm were defined as those with at least one DAPI-positive sperm. Moreover, in a separate group in which 'zona-intact' oocytes were incubated with sperm for 24 h at 37°C and then stained by DAPI, the rate of those oocytes to develop to the two-cell stage was determined under a stereoscopic microscope without fixation.

To count the number of sperm adhered to an oocyte, cumulus cells were dispersed from oocytes in TYH medium containing hyaluronidase (Merk4Biosciences), and the oocytes were denuded of the ZP by incubation in acid Tyrode's solution (Sigma). The C57BL/6N sperm (ca. 1.5×10^5 sperm/ml) were added to a 30-μl drop of TYH medium containing 30 'zona-free' oocytes and then the dish was incubated for 1 h at 37°C. After incubation, the oocytes were fixed with a PFA-GLA-PVP solution and stained with DAPI. The number of sperm adhered to an oocyte was determined by counting DAPI-positive sperm on an oocyte.

Membrane localization of β-catenin before and after membrane adhesion. To observe the localization of β-catenin before and after membrane adhesion, oocytes were collected as mentioned in the 'Determination of litter size and IVF' section. After ZP removal, 'zona-free' oocytes were incubated with C57BL/6N epididymal sperm (ca. 1.5×10^5 sperm/ml) in a 30-μl drop of TYH medium for 30 min at 37°C. The oocytes adhered to sperm, oocytes before sperm adhesion, and epididymal sperm were fixed by placing them in PFA-GLA-PVP solution, washed, and immunostained with a mAb against β-catenin and DAPI, as described in the 'Immunostaining' section.

IVF of oocytes treated with UBE1-41. To study the effect of UBE1-41 on sperm-oocyte fusion, oocytes were collected as mentioned in the 'Determination of litter size and IVF' section, incubated in a 30-μl drop of TYH medium containing UBE1-41 (Biogenova) and DAPI for 1 h at 37°C, and washed with TYH medium. After ZP removal, 'zona-free' oocytes (30 oocytes) were incubated with C57BL/6N epididymal sperm (ca. 1.5×10^5 sperm/ml) in a 30-μl drop of TYH medium for 30 min at 37°C. These oocytes were then fixed by placing them in PFA-GLA-PVP solution, washed, and immunostained with a mAb against β-catenin, as described in the 'Immunostaining' section. The 'zona-free' oocytes were similarly treated in a medium without UBE1-41 and used as the control. The relative rate of oocytes fused with sperm was compared between UBE1-41-treated and untreated oocytes.

1. Ikawa, M., Inoue, N., Benham, A. M., and Okabe, M. Fertilization: a sperm's journey to and interaction with the oocyte. *J Clin Invest* **120**, 984–994 (2010).
2. Mitamura, T. *et al.* The 27-kD diphtheria toxin receptor-associated protein (DRAP27) from vero cells is the monkey homologue of human CD9 antigen: expression of DRAP27 elevates the number of diphtheria toxin receptors on toxin-sensitive cells. *J Cell Biol* **118**, 1389–1399 (1992).
3. Inoue, N., Ikawa, M., Isotani, A., and Okabe, M. The immunoglobulin superfamily protein Izumo is required for sperm to fuse with eggs. *Nature* **434**, 234–238 (2005).
4. Miyado, K. *et al.* Requirement of CD9 on the egg plasma membrane for fertilization. *Science* **287**, 321–324 (2000).
5. Le Naour, F. *et al.*, Severely reduced female fertility in CD9-deficient mice. *Science* **287**, 319–321 (2000).
6. Miyado, K. *et al.* The fusing ability of sperm is bestowed by CD9-containing vesicles released from eggs in mice. *Proc Natl Acad Sci USA* **105**, 12921–12926 (2008).
7. Barraud-Lange, V. *et al.* Transfer of oocyte membrane fragments to fertilizing spermatozoa. *FASEB J* **21**, 3446–3449 (2007).
8. Runge, K. E. *et al.* Oocyte CD9 is enriched on the microvillar membrane and required for normal microvillar shape and distribution. *Dev Biol* **304**, 317–325 (2007).
9. Yamada, S. *et al.* Deconstructing the cadherin-catenin-actin complex. *Cell* **123**, 889–901 (2005).
10. De Vries, W. N. *et al.* Maternal beta-catenin and E-cadherin in mouse development. *Development* **131**, 4435–4445 (2004).
11. Nagafuchi, A., Ishihara, S., and Tsukita, S. The roles of catenins in the cadherin-mediated cell adhesion: functional analysis of E-cadherin-alpha catenin fusion molecules. *J Cell Biol* **127**, 235–245 (1994).
12. Behrens, J. *et al.* Functional interaction of beta-catenin with the transcription factor LEF-1. *Nature* **382**, 638–642 (1996).
13. Fulka, J., Jr., Flechon, B., and Flechon, J. E. Fusion of mammalian oocytes: SEM observations of surface changes. *Reprod Nutr Dev* **29**, 551–557 (1989).

14. Takeichi, M. The cadherins: cell-cell adhesion molecules controlling animal morphogenesis. *Development* **102**, 639–655 (1988).
15. Ziv, S., Rufas, O., and Shalgi, R. Cadherins expression during gamete maturation and fertilization in the rat. *Mol Reprod Dev* **62**, 547–556 (2002).
16. Bedford, J. M., Mori, T., and Oda, S. The unusual state of the cumulus oophorus and of sperm behaviour within it, in the musk shrew, Suncus murinus. *J Reprod Fertil* **110**, 127–134 (1997).
17. Boussadia, O. *et al.* E-cadherin is a survival factor for the lactating mouse mammary gland. *Mech Dev* **115**, 53–62 (2002).
18. Brault, V. *et al.* Inactivation of the beta-catenin gene by Wnt1-Cre-mediated deletion results in dramatic brain malformation and failure of craniofacial development. *Development* **128**, 1253–1264 (2001).
19. Vasioukhin, V. *et al.* Hyperproliferation and defects in epithelial polarity upon conditional ablation of alpha-catenin in skin. *Cell* **104**, 605–617 (2001).
20. Le, T. L., Yap, A. S., and Stow, J. L. Recycling of E-cadherin: a potential mechanism for regulating cadherin dynamics. *J Cell Biol* **146**, 219–232 (1999).
21. Aberle, H. *et al.* Beta-catenin is a target for the ubiquitin-proteasome pathway. *EMBO J* **16**, 3797–3804 (1997).
22. Molfetta, R. *et al.* Lipid raft-dependent FcepsilonRI ubiquitination regulates receptor endocytosis through the action of ubiquitin binding adaptors. *PLoS One* **4**, e5604 (2009).
23. Granell, S., Mohammad, S., Ramanagoudr-Bhojappa, R., and Baldini, G. Obesity-linked variants of melanocortin-4 receptor are misfolded in the endoplasmic reticulum and can be rescued to the cell surface by a chemical chaperone. *Mol Endocrinol* **24**, 1805–1821 (2010).
24. Daniel, J. M. and Reynolds, A. B. The tyrosine kinase substrate p120cas binds directly to E-cadherin but not to the adenomatous polyposis coli protein or alpha-catenin. *Mol Cell Biol* **15**, 4819–4824 (1995).
25. Brind, S., Swann, K., and Carroll, J. Inositol 1,4,5-trisphosphate receptors are downregulated in mouse oocytes in response to sperm or adenophostin A but not to increases in intracellular Ca(2+) or egg activation. *Dev Biol* **223**, 251–265 (2000).
26. Bowerman, B. and Kurz, T. Degrade to create: developmental requirements for ubiquitin-mediated proteolysis during early C. elegans embryogenesis. *Development* **133**, 773–784 (2006).
27. Cheon, S. S. *et al.* beta-Catenin stabilization dysregulates mesenchymal cell proliferation, motility, and invasiveness and causes aggressive fibromatosis and hyperplastic cutaneous wounds. *Proc Natl Acad Sci U S A* **99**, 6973–6978 (2002).
28. Kimura, T. *et al.* The stabilization of beta-catenin leads to impaired primordial germ cell development via aberrant cell cycle progression. *Dev Biol* **300**, 545–553 (2006).
29. Coutifaris, C. *et al.* E-cadherin expression during the differentiation of human trophoblasts. *Development* **113**, 767–777 (1991).
30. Deli, M. A. Potential use of tight junction modulators to reversibly open membranous barriers and improve drug delivery. *Biochim Biophys Acta* **1788**, 892–910 (2009).
31. Jegou, A. *et al.* CD9 tetraspanin generates fusion competent sites on the egg membrane for mammalian fertilization. *Proc Natl Acad Sci U S A* **108**, 10946–10951 (2011).
32. Gamallo, C. *et al.* Correlation of E-cadherin expression with differentiation grade and histological type in breast carcinoma. *Am J Pathol* **142**, 987–993 (1993).
33. Choi, Y. H. and Toyoda, Y.. Cyclodextrin removes cholesterol from mouse sperm and induces capacitation in a protein-free medium. *Biol Reprod* **59**, 1328–1333 (1998).
34. Sakakibara, K. *et al.* Molecular identification and characterization of Xenopus egg uroplakin III, an egg raft-associated transmembrane protein that is tyrosine-phosphorylated upon fertilization. *J Biol Chem* **280**, 15029–15037 (2005).
35. Jones-Villeneuve, E. M., McBurney, M. W., Rogers, K. A., and Kalnins, V. I.. Retinoic acid induces embryonal carcinoma cells to differentiate into neurons and glial cells. *J Cell Biol* **94**, 253–262 (1982).
36. Sato, K. *et al.* Low density detergent-insoluble membrane of Xenopus eggs: subcellular microdomain for tyrosine kinase signaling in fertilization. *Development* **129**, 885–896 (2002).
37. de Vries, W. N. *et al.* Expression of Cre recombinase in mouse oocytes: a means to study maternal effect genes. *Genesis* **26**, 110–112 (2000).

Acknowledgements

We thank W.N. de Vries and B.B. Knowles for the Zp3-Cre transgenic mice. This work was supported by a grant from The Ministry of Health, Labor and Welfare, and grant-in-aid for Scientific Research, The Ministry of Education, Culture, Sports, and Technology of Japan.

Author Contributions

KM conceived and designed the experiments. YT, KY, MS, AN, NK, KS, TK, YH, NO, SK, and MM performed the experiments. HS, YT, HA, and AU analyzed the data. KM wrote the main manuscript text and prepared figures. All authors reviewed the manuscript.

Additional information

Supplementary Information accompanies this paper at http://www.nature.com/scientificreports

Competing financial interests: The authors declare no competing financial interests.

How to cite this article: Takezawa, Y. *et al.* β-catenin is a molecular switch that regulates transition of cell-cell adhesion to fusion. *Sci. Rep.* **1**, 68; DOI:10.1038/srep00068 (2011).

Biochemical and Biophysical Research Communications 410 (2011) 351–357

Contents lists available at ScienceDirect

Biochemical and Biophysical Research Communications

journal homepage: www.elsevier.com/locate/ybbrc

Innate immune system still works at diapause, a physiological state of dormancy in insects

Akihiro Nakamura [a,1], Kenji Miyado [a,*,1], Youki Takezawa [a], Naoko Ohnami [a], Masahiro Sato [b], Chihiro Ono [a], Yuichirou Harada [a], Keiichi Yoshida [a], Natsuko Kawano [a], Seiya Kanai [a], Mami Miyado [a], Akihiro Umezawa [a]

[a] Department of Reproductive Biology, National Center for Child Health and Development, 2-10-1 Okura, Setagaya, Tokyo 157-8535, Japan
[b] Section of Gene Expression Regulation, Frontier Science Research Center, Kagoshima University, 1-21-20 Korimoto, Kagoshima 890-0065, Japan

ARTICLE INFO

Article history:
Received 25 May 2011
Available online 7 June 2011

Keywords:
Innate immune system
Diapause
Hemocyte
Insect
Pupae
Dormancy

ABSTRACT

Diapause is most often observed in insects and is a physiologically dormant state different from other types of dormancy, such as hibernation. It allows insects to survive in harsh environments or extend longevity. In general, larval, pupal, or adult non-diapausing insects possess an innate immune system preventing the invasion of microorganisms into their bodies; however, it is unclear whether this system works under the dormant condition of diapause. We here report the occurrence of innate cellular reactions during diapause using pupae of a giant silkmoth, *Samia cynthia pryeri*. Scanning electron microscopic analysis demonstrated the presence of two major types of cells in the body fluid isolated from the thoracic region of a pupa. Phagocytosis and encapsulation, characteristics of innate cellular reactions, by these cells were observed when latex beads as foreign targets were microinjected into the internal portion of a pupa. Such behavior by these cells was still observed even when pupae were continuously chilled at 4 °C. Our results indicate that innate cellular reactions can work in diapausing insects in a dormant state.

1. Introduction

Insects have evolved a diverse strategy of diapause that occurs at the embryonic, larval, pupal, or adult stage, depending on the species [1]. Initiation of diapause in insects is controlled by different mechanisms, depending on their developmental stage. For example, pupal diapause is regulated by the absence or presence of prothoracicotropic hormone, an insect neurohormone, released from the brain [1]. Adult diapause is induced when juvenile hormone, a hormone secreted by secretory glands located near the brain, is deficient, while larval diapause is induced by juvenile hormone [2]. Once diapause occurs, the respiratory activity of insects drops markedly and the lowered activity is maintained at a minimum level, under which the insects are able to survive for months or even years [3].

In insects, the innate immune system generally consists of humoral and cellular defense reactions [4]. Since this system is a characteristic of plants, fungi, insects, and primitive multicellular organisms (but not for mammals), it has long been considered an evolutionarily older defense system [4]. However, the recent discovery of Toll-like receptors in both insects and mammals provided a new insight into the role of innate immunity as a skillful system for preventing the invasion of microorganisms into the body [5]. The humoral defense reactions are mediated by (1) production of anti-microbial peptides, (2) stimulation of cascades that regulate coagulation and melanization of hemolymph, a body fluid circulating within an insect body like blood in mammals, and (3) production of reactive intermediates of oxygen and nitrogen [6].

Since hemocytes that are similar to blood cells in mammals are known to be present in many insects, such as the silkmoth, *Bombyx mori*, fruit fly, *Drosophila melanogaster*, desert locust, *Schistocerca gregaria*, and sphinx moth, *Manduca sexta*, they are believed to play roles in the innate immune system [7]. Cellular defense reactions, such as "phagocytosis" and "encapsulation" are preceded by two different types of hemocytes, depending on the insect species [7]. For instance, in *Lepidoptera*, granulocytes and plasmatocytes are involved in the reactions, whereas in *Drosophila*, plasmatocytes and lamellocytes are involved [7]. Insect hemocytes can not only recognize and eliminate a variety of foreign targets, but also alter part of their own tissues during metamorphosis, a biological phenomenon required for developing to the next stage in insects [8]. Similarly, in amphibians and mammals, immune cells participate in tissue regeneration by eliminating damaged cells [9]. Several lines of evidence have demonstrated that humoral and cellular defense reactions work coordinately [10]. In addition, cross-talk between the immune and nervous systems is thought to

* Corresponding author. Fax: +81 3 5494 7048.
E-mail address: kmiyado@nch.go.jp (K. Miyado).
[1] These authors equally contributed to this work.

0006-291X/$ - see front matter © 2011 Elsevier Inc. All rights reserved.
doi:10.1016/j.bbrc.2011.06.015

be important for regulating inflammation-like reactions upon microbial infection [11]; however, little is known about hemocyte-mediated cellular defense reactions at diapause. In this study, we explored the above possibility using diapausing pupae of a giant moth, *Samia cynthia pryeri*, inhabiting a field.

2. Materials and methods

2.1. Animals

Fifty diapausing pupae of *S. cynthia pryeri* (about 2 months after pupation) were collected from an outdoor rearing location in a field near Matsumoto city (Nagano, Japan) in early December, and stored in an incubator at 4 °C until used for experiments. Since a male pupa is bigger than a female pupa, the former is superior for isolation of a relatively large amount of body fluid (in which innate immunity-related cells are supposed to be included) than the latter. Based on this reason, we used male pupae (3–5 months after pupation) throughout the following experiments.

2.2. Identification of hemocyte-like cells in diapausing pupae

Hemocyte-like cells were identified as described in supplementary content.

2.3. Determination of respiration rates in diapausing pupae

Respiration rates were measured as described in supplementary content.

2.4. Analysis by scanning electron microscopy (SEM)

Hemolymph collected from a diapausing pupa was observed as described in supplementary content.

2.5. Injection of latex beads into diapausing pupae

To monitor the behavior of innate immunity-related cells probably present within diapausing pupae, microinjection experiments were performed as described in supplementary content.

3. Results

3.1. Life cycle of S. cynthia pryeri

The Ailanthus silkmoth, *S. cynthia*, is a saturniid moth used to produce silk fabric, but is not so domesticated as the silkworm, *B. mori*. In Japan, a subspecies of *S. cynthia* exists and is named *S. cynthia pryeri*. This insect is often called "eri-silkmoth" as its common name, because it feeds on the leaves of the castor bean and produces eri-silk. The name 'eri' is derived from the Assamese word 'era', which means castor. Eri-silk is extremely durable, but cannot be easily reeled off the cocoon and is thus spun like cotton or wool. Under cold climatic conditions (from November to June), *S. cynthia pryeri* sleep as a diapausing pupa and then develop to a moth in early summer (Fig. 1A). The moth has very large wings, 113–125 mm in length, with whitish and yellow stripes against a brown background (Fig. 1B). The pupa does not change its morphology or weight during the long diapausing period, and males are larger than females (Fig. 1C).

Under laboratory conditions, diapausing pupae can survive for over a year without awakening from diapause, as long as they are continuously stored at 26 °C. For development of a pupa to a moth, the diapausing pupa must be exposed to low temperature (under 4 °C) for over 90 days and subsequently warmed at 26 °C. As shown in Fig. 1D, in pupae exhibiting complete diapause, transient spike-like CO_2 discharge is seen, indicating that their metabolic activity drops markedly and their dormant condition is properly maintained. In this study, male pupae exhibiting a spike-like respiration pattern were defined as those in complete diapause and were used in the following experiments.

3.2. Presence of innate immunity-related cells in diapausing pupae

To assess possible evidence for the occurrence of innate immune reactions at diapause, we first explored the presence of cells that appear to be similar to hemocytes in diapausing pupae of *S. cynthia pryeri*. Prior to this investigation, we selected diapausing pupae exhibiting complete diapause. Since the respiratory activity of a pupa reaches the minimum level by 15 days after pupation (initiation of cocoon formation), it is thought that stable diapause is achieved more than 15 days after pupation; therefore, we used diapausing pupae 90–150 days after pupation in this experiment. Furthermore, it is important to know where hemocytes reside within a diapausing pupa. Hemocytes are thought to not only be involved in cellular defense reactions, but also in tissue formation via metamorphosis [8]. Based on this knowledge, we supposed that pupal hemocytes reside around immature organs, such as wing imaginal discs, to participate in the forthcoming metamorphosis after diapause. We thus collected body fluid from the thoracic region of diapausing pupa where wing imaginal discs are located (Fig. 2A). Light microscopic observation of cellular content included in the collected body fluid revealed that all (10 tested) of the diapausing pupae had cells free from tissues (Fig. 2B). These cells were divided into two major types: Type I cells (arrows in Fig. 2B) were ca. 10 μm in diameter, round and less adhesive, and exhibited low migrating ability; Type II cells (arrowheads in Fig. 2B) were more than 20 μm in diameter, flat and adhesive, and exhibited high migrating ability. The rates of Type I and II cells in the collected body fluid were 47.3 ± 1.8% and 46.8 ± 2.2%, respectively (Fig. 2C). In addition to these two types of cells, there was a minor type of sticky cell (ca. 10 μm in diameter) that was categorized as "others" in Fig. 2C.

To examine these two cell types in more detail, we performed SEM analysis. As already noted from light microscopic analysis, there were two distinct types of cells. One exhibited round morphology and protruding microvillar processes (upper panels of Fig. 2D), corresponding to Type I cells (arrows in Fig. 2B) observed under a light microscope. The other exhibited flattened morphology and extended peripheral waves similar to lamellipodia (lower panels of Fig. 2D), corresponding to the previous Type II cells (arrowheads in Fig. 2B). Type I cells (9.0 ± 0.3 μm) were smaller than Type II cells (26.8 ± 1.0 μm) in average diameter. These Type I and II cells shared morphological features with granulocytes and plasmatocytes, respectively, identified as insect hemocytes in a sphinx moth, *M. sexta* [7]. These results indicate the presence of at least two types of cells similar to hemocytes in the diapausing pupae of *S. cynthia pryeri*.

3.3. Responses of hemocyte-like cells to foreign latex beads in vivo

As mentioned previously, two cell types similar to hemocytes were found in a diapausing pupa of *S. cynthia pryeri*. To examine whether these cells exhibit defensive ability against foreign invaders, latex beads were microinjected as a target of the cellular reaction into the right side of the thoracic ventral region of a pupa incubated at 20 °C using a glass microcapillary, as depicted in Fig. 3A. Six hours after injection, the injected beads were recovered by suctioning the internal body fluid (10 μl) through the left side of the thoracic ventral region of the bead-injected pupa using a glass

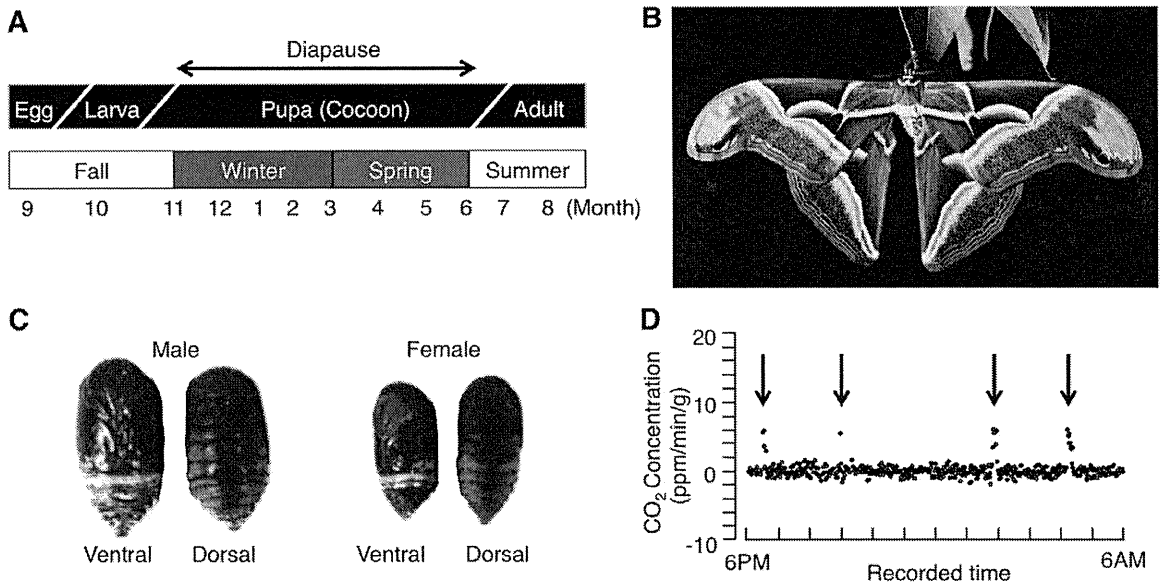

Fig. 1. Features of diapausing pupae of a giant moth, *Samia cynthia pryeri*. (A) Life cycle of the insect. The most common life cycle is univoltine, in which this moth takes one year to complete its life, winters as a diapausing pupa, and then develops to an adult in early summer. Notably, the pupa spends more than 6 months in diapause. (B) Male moth. The moth has large wings (ca. 120 mm in width) with whitish stripes and a brown background on both the upper and lower wings. (C) Diapausing pupae. Left image: male pupa; right image: female pupa. (D) Representative pattern of transient, spike-like CO_2 discharge (indicated by arrows) in the diapausing pupa 30 days after pupation. Periodic appearance of spike-like CO_2 discharge indicates a marked decrease in metabolic activity and normal diapausing conditions.

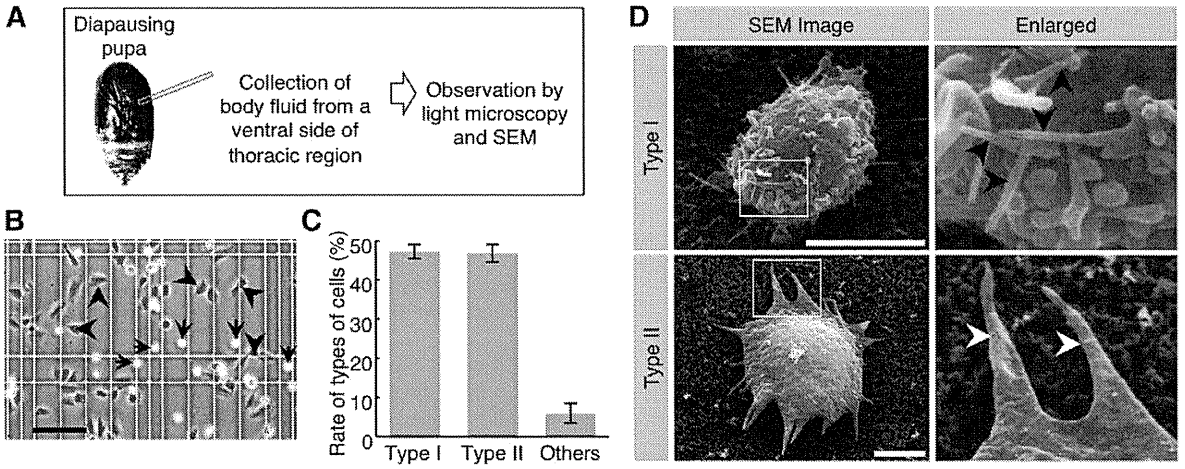

Fig. 2. Discovery of hemocyte-like cells in diapausing pupae. (A) Experimental design. Since pupal hemocytes were predicted to reside around wing imaginal discs, body fluid was collected for microscopic analysis from thoracic regions that house wing imaginal discs. (B) Hemocyte-like cells present in the body fluid collected from the thoracic region of a pupa. Arrows and arrowheads indicate Type I and II cells, respectively. Scale bars: 50 μm. (C) Rate of hemocyte-like cells (classified as Type I, Type II and others) in body fluids collected from the thoracic region shown in B. Over 2000 cells were counted. The rate of each cell type is determined and expressed as a percentage of a target cell type among the total number of cells counted in ten quadrants (1 mm × 1 mm in square). Values are the mean ± standard error (SE). (D) SEM analysis of migrating cells in the diapausing pupae of *Samia cynthia pryeri*. The migrating cells collected from the thoracic region of diapausing pupae of *Samia cynthia pryeri* were subjected to SEM analysis. Right panels are enlarged images of insets in the left panels. Black arrowheads: microvillus-like structures elongated from Type I cells; white arrowheads: lamellipodia-like structures extended from Type II cells. Scale bars: 10 μm.

microcapillary. The cellular content included in the recovered body fluid was then subjected to SEM analysis (Fig. 3B–E).

As expected, the two cell types shown in Fig. 2D were seen in the cellular content (marked by arrowhead and asterisks in Fig. 3B). Notably, only one (marked by asterisks) of the two cell types exhibited phagocytotic behavior toward the foreign beads (Fig. 3C). In some cases, two or more cells were engulfing a bead (Fig. 3D). These cells exhibited round morphology with microvilli and their average diameter was ca. 10 μm (Fig. 3B–D). These features clearly match those of Type I cells, shown in Fig. 2D. On the other hand, the capsule was detected in the cellular content (Fig. 3E). Since *Lepidoptera* granulocytes and plasmatocytes are involved in encapsulation [7], another type of lamellipodial cell, morphologically similar to plasmatocytes [7], is supposed to exhibit behavior (namely, encapsulation) different from that of Type I cells (Fig. 3E). These cells have a larger diameter and flat cell surface, suggesting a feature of the Type II cells shown in Fig. 2D. Concomitantly, hemolymph containing injected beads was smeared on the glass slides for Giemsa staining. Similar to the findings obtained from SEM analysis, phagocytosis (Fig. 3F) and encapsulation

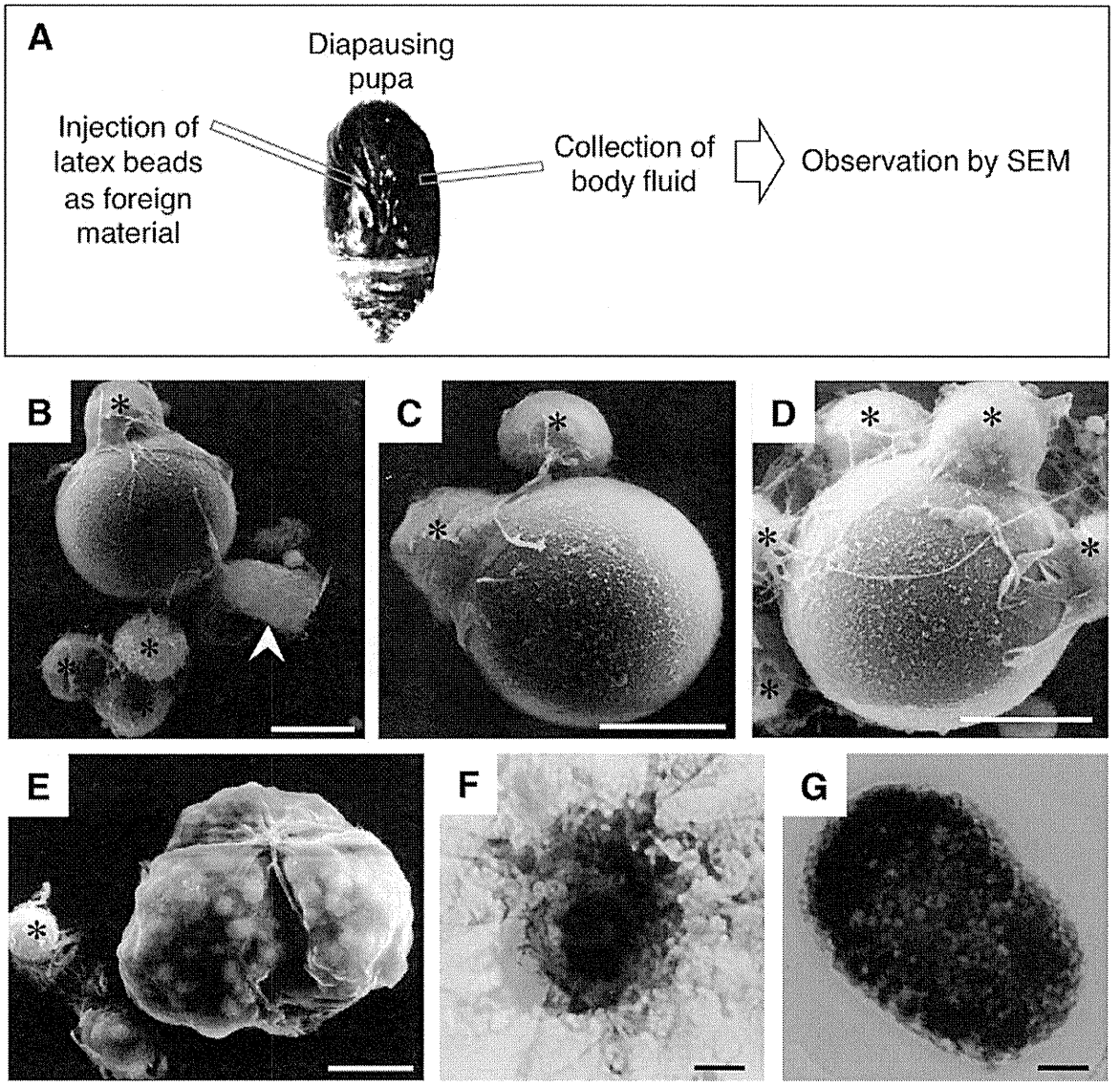

Fig. 3. Innate immune reactions as revealed by microinjection of foreign latex beads into diapausing pupae of *Samia cynthia pryeri*. (A) Experimental design. To assess the behavior of hemocyte-like cells toward foreign targets, latex beads were microinjected into the right side of the thoracic ventral region of a pupa incubated at 20 °C using a glass microcapillary. Six hours after injection, the beads were recovered by suctioning the body fluid from the left side of the thoracic ventral region. (B) Two types of hemocyte-like cells adhered to the injected latex bead. Black asterisks and white arrowhead indicate Type I and II cells, respectively. (C) Type I cells (indicated by asterisks) displaying phagocytotic behavior against the bead. (D) Five Type I cells (indicated by asterisks) displaying phagocytotic behavior against the bead. (E) Type II cells encapsulating bead. Type I cells (indicated by asterisks) are present near the encapsulated bead. (F) Giemsa staining indicating phagocytosis by Type I cells. Note the presence of Type I cells stained blue surrounding the black bead. (G) Giemsa staining indicating encapsulation by Type II cells. Note that the black bead is completely surrounded by blue-stained Type II cells. Scale bars: 10 μm.

(Fig. 3G) were observed. From these collective results, migrating cells found in a diapausing pupa have defensive abilities, as exemplified by their phagocytosis and encapsulation, suggesting that innate cellular reactions work even in diapause.

3.4. Cellular responses under low-temperature

During the winter season where *S. cynthia pryeri* inhabits, the outdoor temperature is usually below 0 °C throughout the day. As a result, microorganisms such as bacteria and fungi become metabolically inactive, although they are still alive and can grow slowly [12]. Furthermore, they often suffer from bacterial invasion [13]; however, it is still unknown whether the innate immune system works in diapausing pupae exposed to low temperature (4 °C or below).

To assess the question, we examined the defensive ability of diapausing pupae stored at 4 °C by microinjecting latex beads into their internal lumen, as depicted in Fig. 3A. After injection, the injected beads were recovered by sucking out the body fluid each hour and subjecting it to Giemsa staining to identify innate immunity-related cells. In pupae incubated at 20 °C, phagocytosis by Type I cells was observed in all the samples tested, which had been collected up to 5 h after bead injection. Furthermore, the number of beads phagocytosed increased in a time-dependent manner (upper left graph in Fig. 4). In pupae incubated at 4 °C, phagocytosis was still observed, but the frequency was lower than in pupae incubated at 20 °C (upper right graph in Fig. 4). In contrast, the average rates of encapsulation were below 10% in both groups when samples were examined up to 5 h after bead injection (mid-

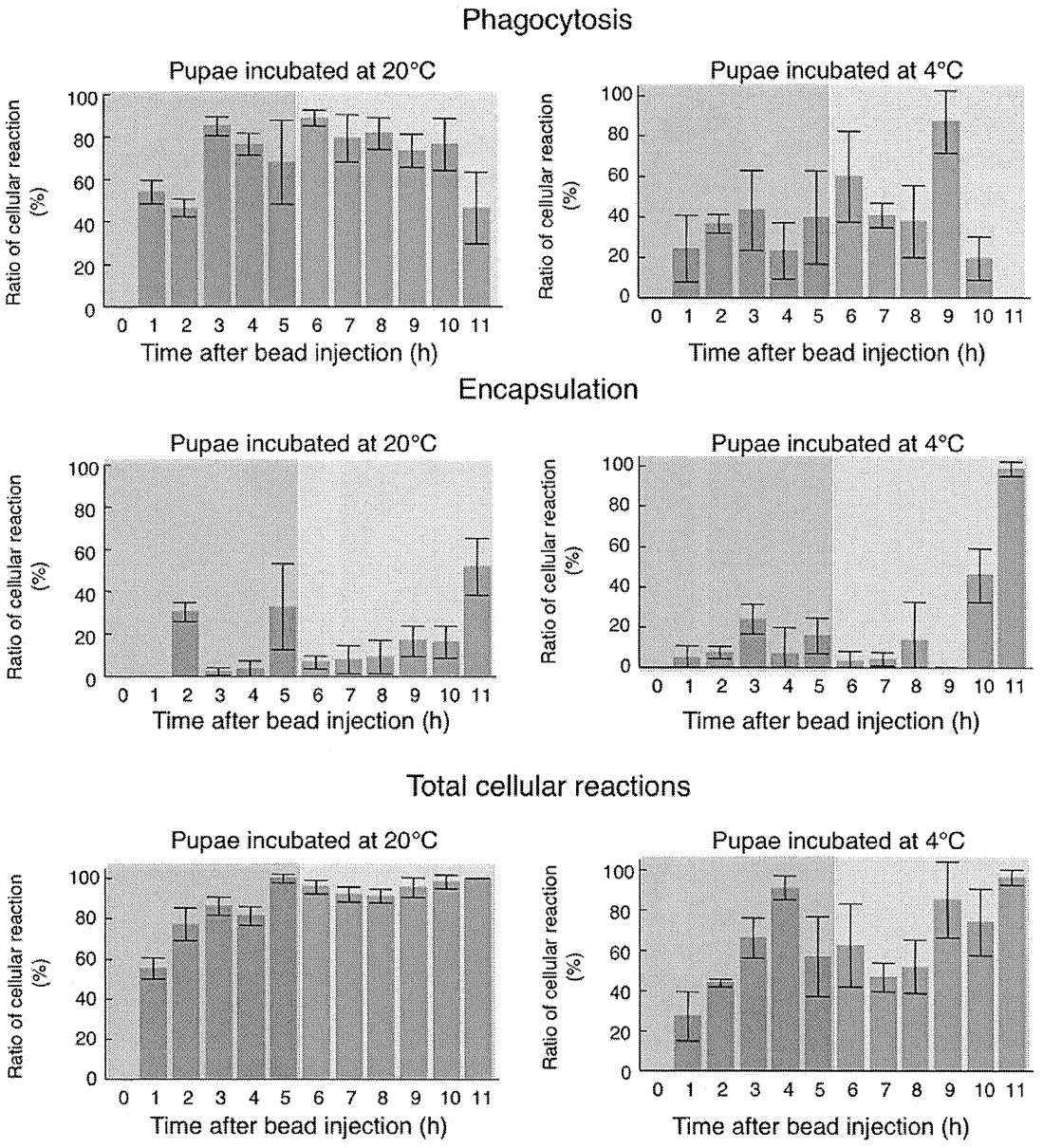

Fig. 4. Cellular defense reactions in diapausing pupae incubated at two different temperatures. As depicted in A, latex beads were microinjected into the right side of thoracic ventral region of a diapausing pupa incubated at 4 or 20 °C, and then the injected beads were recovered from the left side of the thoracic ventral region each hour after bead injection. Phagocytosis and encapsulation were evaluated by inspecting specimens after Giemsa staining. The rate of each cellular defense reaction was determined as described in Fig. 2C. Total cellular reactions were determined by the sum of the rates of phagocytosis and encapsulation.

dle graphs in Fig. 4). The degree of total cellular reactions in the group treated at 4 °C was low compared to the group treated at 20 °C (lower graphs in Fig. 4). These results suggest that the innate immunity associated with phagocytosis and encapsulation is affected by temperature outside the insect bodies.

Similar results were obtained when phagocytotic activities were evaluated 6–11 h after bead injection (upper graphs in Fig. 4). Notably, the encapsulation rate tended to gradually increase in pupae incubated at 4 °C and reached at the maximal level of 95.0 ± 0.4% at 11 h after bead injection. This is in contrast with the rate (50.0 ± 0.6%) in pupae incubated at 20 °C (middle graphs in Fig. 4). These results suggest that the phagocytotic activity of Type I cells is affected by outside temperature, while encapsulation by Type II cells proceeds even at low temperature (4 °C). This means that innate cellular reactions still work in diapausing pupae exposed to low temperature.

4. Discussion

Insects overcome harsh environmental conditions, such as food shortages and extremely low or high temperatures, by employing a unique system, termed diapause [1]. For example, in the case of pupal diapause, at which stage food sources are unavailable, managing the metabolic resources stored in their bodies is critical for their survival [1]. Metabolic depression, as represented by spike-like respiration (shown in Fig. 1D), is one of the strategies for insects to promote reserve conservation [1]. Diapausing insects also

have to control water loss, since they are unable to take in water, especially in the winter season. The body fluid of diapausing insects in this season is viscous and rich in anti-freezing materials, such as glycerol [14]. These properties may protect insects from environmental changes, such as chilling and water shortage. It is also conceivable that diapausing insects may have strategies to protect against bacterial invasion, although the self-defense mechanism remains unknown. Our present study addressed this problem and demonstrated using diapausing pupae of *S. cynthia pryeri* that cellular defense reactions work in diapausing pupae constantly exposed to chilling temperature.

There is much evidence that insects exhibit their immune competence in a non-diapausing state. For example, in non-diapausing adults of *D. melanogaster*, temperature-induced changes in immune competence are accompanied with cell surface alterations that cause their hemocytes to adhere and encapsulate a parasite [15]. At 29 °C, the hemocytes can encapsulate eggs of the parasitic wasp, but they are essentially immune incompetent at 21 °C [15]. In addition to terrestrial insects, marine invertebrates have their own innate immune system [16]. In sea cucumber, *Apostichopus japonicus*, acute temperature change significantly affects phagocytosis, but not encapsulation [17]. This evidence suggests that innate cellular reactions are sensitive to temperature change, and phagocytosis appears to be more susceptible to this change than encapsulation. We also noted that phagocytosis is more susceptible to low temperature than encapsulation in diapausing pupae of *S. cynthia pryeri* (see Fig. 4).

Bead injection into the internal portion of a pupa has been proven as a simple and effective approach to evaluate cellular immune reactions *in vivo* [18]. This direct approach is particularly valuable when the genetic background and species of the target samples is unknown. In this case, the collected body fluid containing injected beads was always analyzed by electron microscopy, such as SEM; however, SEM is labor-intensive and requires a relatively long time to obtain results. Giemsa staining of smeared body fluid was found to be useful for rapid identification of innate immunity-related cells in this study, as shown in Fig. 3F, G. Thus, Giemsa staining would be beneficial for routine identification of innate immunity-related cells recovered after bead injection. Flow cytometric analysis is also a useful alternative to identify and purify blood cells of various animals, including *D. melanogaster* [19]. For this, it requires specific lectins or antibodies recognizing those cells. In fact, lectin-like substances with hemagglutinating activity have been found in the hemolymph of a variety of insect species [8]. In some insects, lectin-binding patterns correlate with the immune capabilities of the hemocytes [20]. Unfortunately, neither lectin nor an antibody that specifically recognizes hemocytes derived from *S. cynthia pryeri* is available.

The number of hemocytes has been estimated in diapausing and non-diapausing larvae of the greater sugar cane borer, *Sesamia cretica* [21]. During diapause, the number of each type of hemocyte is significantly reduced, but it increases along with termination of diapause, suggesting the possible incompetence of innate cellular reactions at diapause [21]. However, our present results obtained from injecting latex beads demonstrated that cellular defense reactions continue to function in diapausing pupae of *S. cynthia pryeri*. This indicates that the activity of the innate cellular system is reduced in diapause, but is maintained.

SEM analysis of cells included in body fluid of diapausing *S. cynthia pryeri* demonstrated the presence of two major types of hemocytes, termed Type I and II cells. Minor types of cells (ca. 10 μm in diameter), which are sticky and categorized as "others" in Fig. 2C, were also detected. The morphological features of Type I cells are similar to those of granulocytes in *Lepidoptera* [7]. Granulocytes are known to differentiate into other types of cells [22]. Probably, the minor types of cells mentioned above are derived from Type I cells.

To date, the presence of seven subpopulations of hemocytes has been reported in several insect species, but not all of these subpopulations are always present in each species [7]. The most common types of hemocytes are prohemocytes, plasmatocytes, granulocytes, spherulocytes, adipocytes, and oenocytoids, although each cell type slightly differs among species. Notably, close similarity of immunological functions has been demonstrated between vertebrate leukocytes and insect hemocytes [23]. For example, prohemocytes, plasmatocytes and granulocytes are thought to correspond to lymphocytes, monocytes and neutrophils in humans, respectively [23]. The kinetics of phagocytosis and microbial killing is similar between insects and humans [23]. For precise characterization of the hemocyte subpopulation, the development of appropriate cell surface markers for segregating each type of hemocyte subpopulation will be required.

At present, little is known about the molecular mechanism underlying the induction and maintenance of insect diapause. Emerson et al. [1] suggest that the induction and maintenance of larval or pupal diapause are under direct control of the insect brain via neuro-endocrine complex. As previously mentioned, diapause is beneficial for insects to survive under severe environmental conditions and to extend their longevity. In this context, further understanding of the nature of insect diapause will provide new insight into studies on human longevity, pathogenesis and the development of therapeutic drugs.

In conclusion, we show for the first time using a bead injection method into the internal portion of a pupa that cellular defense reactions work even in diapausing pupae of *S. cynthia pryeri*, which are continuously exposed to chilling temperature. This finding would be useful to further understand the role of hemocytes in insect innate immunity.

Acknowledgments

We thank A. Koenuma, K. Mizukoshi, Y. Shinohara, S. Kobayashi and T. Shimada for critical suggestions. This work was supported by a grant from the Ministry of Health, Labor and Welfare, and a grant-in-aid for Scientific Research from the Ministry of Education, Culture, Sports, and Technology of Japan.

Appendix A. Supplementary data

Supplementary data associated with this article can be found, in the online version, at doi:10.1016/j.bbrc.2011.06.015.

References

[1] K.J. Emerson, W.E. Bradshaw, C.M. Holzapfel, Complications of complexity: integrating environmental, genetic and hormonal control of insect diapause, Trends Genet. 25 (2009) 217–225.
[2] H. Numata, S. Nakayama, J. Matsuo, Role of the corpus allatum in the control of adult diapause in the blow fly, Protophormia terraenovae, J. Insect Physiol. 43 (1997) 211–216.
[3] L. Ding, Y. Li, M. Goto, Physiological and biochemical changes in summer and winter diapause and non-diapause pupae of the cabbage armyworm, Mamestra brassicae L. during long-term cold acclimation, J. Insect Physiol. 49 (2003) 1153–1159.
[4] D. Hultmark, Immune reactions in Drosophila and other insects: a model for innate immunity, Trends Genet. 9 (1993) 178–183.
[5] K. Takeda, S. Akira, Toll-like receptors in innate immunity, Int. Immunol. 17 (2005) 1–14.
[6] J.A. Hoffmann, Innate immunity of insects, Curr. Opin. Immunol. 7 (1995) 4–10.
[7] M.D. Lavine, M.R. Strand, Insect hemocytes and their role in immunity, Insect Biochem. Mol. Biol. 32 (2002) 1295–1309.
[8] S. Natori, H. Shiraishi, S. Hori, A. Kobayashi, The roles of Sarcophaga defense molecules in immunity and metamorphosis, Dev. Comp. Immunol. 23 (1999) 317–328.

[9] L.A. Rollins-Smith, Metamorphosis and the amphibian immune system, Immunol. Rev. 166 (1998) 221–230.
[10] J.A. Hoffmann, The immune response of Drosophila, Nature 426 (2003) 33–38.
[11] N. Silverman, Flies kNOw how to signal, Dev. Cell 4 (2003) 5–6.
[12] N.J. Russell, Cold adaptation of microorganisms, Philos. Trans. R. Soc. Lond. B Biol. Sci. 326 (1990) 595–608. discussion 608-11.
[13] G.D. Inglis, A.M. Lawrence, F.M. Davis, Pathogens associated with southwestern corn borers and southern corn stalk borers (Lepidoptera: Crambidae), J. Econ. Entomol. 93 (2000) 1619–1626.
[14] H. Chino, L.I. Gilbert, Diglyceride release from insect fat body: a possible means of lipid transport, Science 143 (1964) 359–361.
[15] A.J. Nappi, M. Silvers, Cell surface changes associated with cellular immune reactions in Drosophila, Science 225 (1984) 1166–1168.
[16] J. Robalino, C.L. Browdy, S. Prior, A. Metz, P. Parnell, P. Gross, G. Warr, Induction of antiviral immunity by double-stranded RNA in a marine invertebrate, J. Virol. 78 (2004) 10442–10448.
[17] F. Wang, H. Yang, F. Gao, G. Liu, Effects of acute temperature or salinity stress on the immune response in sea cucumber, Apostichopus japonicus, Comp. Biochem. Physiol. A Mol. Integr. Physiol. 151 (2008) 491–498.
[18] H. Wago, Cellular recognition of foreign materials by Bombyx mori phagocytes: I. Immunocompetent cells, Dev. Comp. Immunol. 6 (1982) 591–599.
[19] M. Ramet, P. Manfruelli, A. Pearson, B. Mathey-Prevot, R.A. Ezekowitz, Functional genomic analysis of phagocytosis and identification of a Drosophila receptor for E. Coli, Nature 416 (2002) 644–648.
[20] J. Ao, E. Ling, X.Q. Yu, Drosophila C-type lectins enhance cellular encapsulation, Mol. Immunol. 44 (2007) 2541–2548.
[21] M.B. el-Mandarawy, Effects of insect diapause and parasitization of a braconid, Bracon brevicornis Wesm. On the haemolymph of its host Sesamia cretica led, J. Egypt Soc. Parasitol. 27 (1997) 805–815.
[22] J. Rodrigues, F.A. Brayner, L.C. Alves, R. Dixit, C. Barillas-Mury, Hemocyte differentiation mediates innate immune memory in Anopheles gambiae mosquitoes, Science 329 (2010) 1353–1355.
[23] J. Krzemien, L. Dubois, R. Makki, M. Meister, A. Vincent, M. Crozatier, Control of blood cell homeostasis in Drosophila larvae by the posterior signalling centre, Nature 446 (2007) 325–328.

Genes to Cells

Lectin microarray analysis of pluripotent and multipotent stem cells

Masashi Toyoda[1], Mayu Yamazaki-Inoue[1], Yoko Itakura[2], Atsushi Kuno[2], Tomohisa Ogawa[3], Masao Yamada[3], Hidenori Akutsu[1], Yuji Takahashi[1], Seiichi Kanzaki[1], Hisashi Narimatsu[2], Jun Hirabayashi[2] and Akihiro Umezawa[1]*

[1]*Department of Reproductive Biology, National Institute for Child Health and Development, 2-10-1 Okura, Setagaya-ku, Tokyo 157-8535, Japan*

[2]*Research Center for Medical Glycoscience, National Institute of Advanced Industrial Science and Technology, AIST Tsukuba Central 2, Tsukuba, Ibaraki 305-8568, Japan*

[3]*GP BioSceinces Ltd, 1-3-3, Azamino-Minami, Aoba-ku, Yokohama, Kanagawa 225-0012, Japan*

Stem cells have a capability to self-renew and differentiate into multiple types of cells; specific markers are available to identify particular stem cells for developmental biology research. In this study, we aimed to define the status of somatic stem cells and the pluripotency of human embryonic stem (hES) and induced pluripotent stem (iPS) cells using a novel molecular methodology, lectin microarray analysis. Our lectin microarray analysis successfully categorized murine somatic stem cells into the appropriate groups of differentiation potency. We then classified hES and iPS cells by the same approach. Undifferentiated hES cells were clearly distinguished from differentiated hES cells after embryoid formation. The pair-wise comparison means based on 'false discovery rate' revealed that three lectins -*Euonymus europaeus* lectin (EEL), *Maackia amurensis* lectin (MAL) and *Phaseolus vulgaris* leucoagglutinin [PHA(L)]- generated maximal values to define undifferentiated and differentiated hES cells. Furthermore, to define a pluripotent stem cell state, we generated a discriminant for the undifferentiated state with pluripotency. The discriminant function based on lectin reactivities was highly accurate for judgment of stem cell pluripotency. These results suggest that glycomic analysis of stem cells leads to a novel comprehensive approach for quality control in cell-based therapy and regenerative medicine.

Introduction

Stem cells produce almost every tissue of the human body. In general, they have the ability to divide and self-renew and to differentiate into various cell types. Stem cells have varying degrees of differentiation potential: (i) totipotency (ability to form the embryo and the trophoblast of the placenta) like fertilized eggs (zygotes); (ii) pluripotency (ability to differentiate into almost all cells that arise from the three germ layers) like human embryonic stem (hES) cells and induced pluripotent stem (iPS) cells; (iii) multipotentiality (capability of producing a limited range of differentiated cell lineages upon their location) like most tissue-based stem cells; and (iv) unipotentiality (ability to generate one cell type) like cells such as the epidermal stem cells and the spermatogonial cells of the testis. That is, a hierarchy of stem cells exists. In addition, human ES cell lines show variation in differentiation propensity (Osafune *et al.* 2008). iPS cells, another type of pluripotent stem cell, have been generated from somatic cells of different origin by retroviral transduction of four transcription factors (Takahashi *et al.* 2007; Yu *et al.* 2007). The established iPS cells have a wider variety of differentiation ability and gene expression when compared to ES cells (Aoi *et al.* 2008; Lee *et al.* 2009; Kaichi *et al.* 2010). However, a small proportion of these stem cells sometimes show spontaneous differentiation during serial passage. Therefore, to realize the potential for iPS cells to be utilized for cell therapy and as a valuable tool for drug discovery, it is necessary to monitor the status of these stem cells and to define

Communicated by: Takashi Tada
**Correspondence*: umezawa@1985.jukuin.keio.ac.jp

DOI: 10.1111/j.1365-2443.2010.01459.x

their exact stage during processes of growth and/or differentiation.

Glycosylation is a critical post- or co-translational modification found in more than 50% of eukaryotic proteins (Budnik *et al.* 2006). Thus, the glycome, which represents the total set of glycans expressed in a cell, is believed to be information-rich, as it varies among cell types, stages of development and differentiation, and even in the malignant transformation processes (Varki 1993). Lectins have long been used as tools to characterize cell surface glycans, such as for blood-group typing, tissue staining, lectin-probed blotting and flow cytometry (Sharon & Lis 2004). The use of lectins in glycan profiling provides considerable advantages. A modern technology to discriminate glycan profiling is lectin microarray analysis, which is an emerging technology that enables ultrasensitive detection of multiplex lectin–glycan interactions (Angeloni *et al.* 2005; Kuno *et al.* 2005; Pilobello *et al.* 2005). The system developed by Kuno *et al.* (2005) is based on a unique principle, that is, the evanescent-field fluorescence-detection principle, which has been used extensively for biosensors to study real-time binding events on the glass slide surfaces. Thus, the evanescent-field methods have greater advantage to analyze relatively weak interactions between lectins and glycoproteins in a liquid phase at equilibrium. Furthermore, this method is applicable for the analysis of the physiological and pathological status of crude glycoproteins extracted from mammalian cells (Ebe *et al.* 2006; Kuno *et al.* 2008) and cell surfaces (Tateno *et al.* 2007). Although the number of probes in lectin microarray is much smaller than in mRNA expression arrays, lectin microarray analysis enables high-throughput and sensitive analysis of a large set of biological samples and provides a snapshot of cell profiling. In this study, we further developed lectin microarray technology to define the status of somatic and pluripotent stem cells. The glycan-based comprehensive approach promises to be of great value, complementing more established methods such as gene expression analysis and epigenetic analysis.

Results

Lectin microarray analysis of mouse mesenchymal cells

Mesenchymal stem cells are multipotent and therefore may be useful in cell-based therapy along with ES cells and iPS cells. Mesenchymal stem cell (MSC) lines [(9-15c), osteoblasts (KUSA-A1), chondroblasts (KUM5) and preadipocytes (H-1/A)] were established from mouse bone marrow and were shown to retain potency both *in vivo* and *in vitro* (Umezawa *et al.* 1991; Matsumoto *et al.* 2005; Sugiki *et al.* 2007). To investigate their carbohydrate structures, we carried out a lectin microarray analysis of the cell membrane proteins. We quantified lectin signal using 'Array-Pro Analyzer' software and calculated the average net intensities of three spots for each lectin on the chip (Fig. 1A). Experiments with each cell line were performed in triplicate or quadruplicate. Four mesenchymal cell lines with different potencies showed differential lectin reactivities. 9-15c MSCs showed strong reactivity to wheat germ agglutinin (WGA), *Lycopersicon esculentum* lectin (LEL), concanavalin A (ConA), *Sambucus nigra* agglutinin (SNA) and *Ricinus communis* agglutinin I (RCA120) (Fig. 1A and Fig. S1 in Supporting Information). These signal intensities by lectin microarray were consistent with mean fluorescent intensities by flow cytometric analysis (Fig. 1B). We then performed hierarchical clustering analysis and principal component analysis (PCA) on the signal values of each lectin (Fig. 1C, D). H-1/A preadipocytes can be distinguished by KUM5 chondroblasts by lectin reactivities of GSL1A4, GSL1B4, BPL, PWM and MPA (PC1 axis), and 9-15c MSCs can be distinguished by KUSA-A1 osteoblasts by SNA. These cell types were reproducibly categorized into independent distinct groups.

Lectin microarray analysis of human mesenchymal cells

Human MSCs harvested from a variety of tissues have the capability to differentiate into numerous tissue lineages despite the fact that they may have tissue-specific characteristics. To clarify relationship between the tissue-specific characters of mesenchymal cells and glycomics, we performed lectin microarray analysis (LecChip™: Fig. S1 in Supporting Information) of mesenchymal cells derived from various tissues (Fig. 2A). Signal intensities by lectin microarray were consistent with the mean fluorescent intensities analysis determined by flow cytometric analysis (Fig. 2B). Hierarchical clustering analysis showed that human embryonic carcinoma NCR-G3 cells were reproducibly categorized into an independent group (red color in Fig. 2C), which is distinct from a group of mesenchymal cells derived from a variety of tissues (green color in Fig. 2C). In mesenchymal cells, bone marrow-, placenta- and extra finger-derived mesenchymal cells were categorized into distinct groups labeled in yellow, orange and blue, respectively (Fig. 2C).

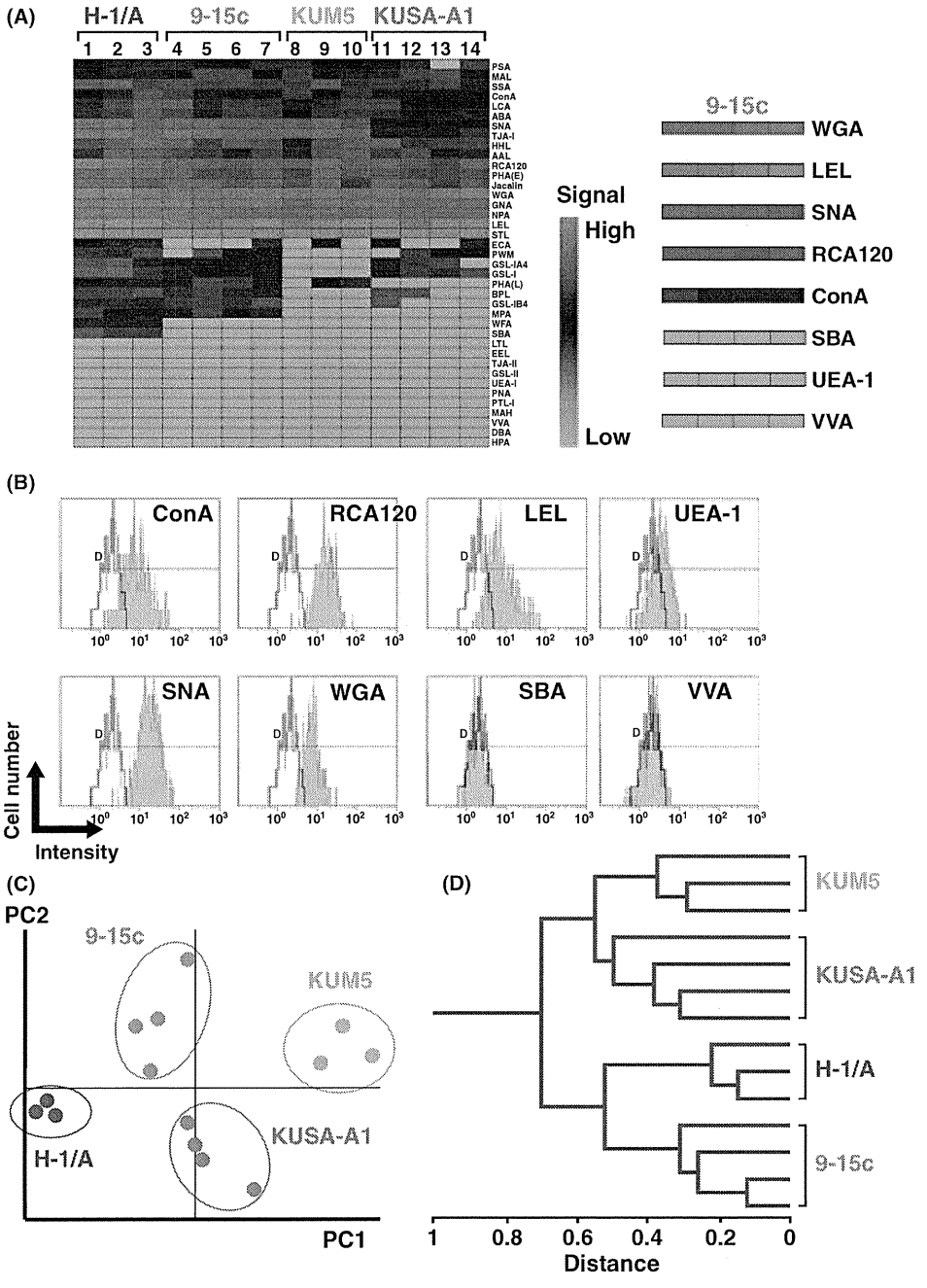

Figure 1 Lectin microarray analysis of mouse mesenchymal cells. (A) Heat map of 9-15c multipotent cells, KUSA-A1 osteoblasts, KUM5 chondroblasts and H-1/A preadipocytes. (B) Flow cytometric analysis of 9-15c multipotent cells using each lectin probe. Mean fluorescent intensities by flow cytometric analysis are consistent with signal intensities by lectin microarray. Nonshaded and shaded areas indicate reactivity of antibodies for isotype controls and that of antibodies for cell surface markers, respectively. (C) Principal component analysis of lectin microarray on mouse bone marrow–derived mesenchymal cells. Each cell is reproducibly subcategorized into groups of mesenchymal cell types. (D) Hierarchical clustering analysis of lectin microarray on mouse bone marrow–derived mesenchymal cells.

Human mesenchymal cells reacted to (i) *Pisum sativum* agglutinin (PSA), *Lens culinaris* agglutinin (LCA), *Aspergillus oryzae* lectin (AOL) and *Aleuria aurantia* lectin (AAL) that bind to Fucα1-6GlcNAc; (ii) SNA, *Sambucus sieboldiana* agglutinin (SSA) and *Trichosanthes japonica* agglutinin I (TJA-I) that bind to

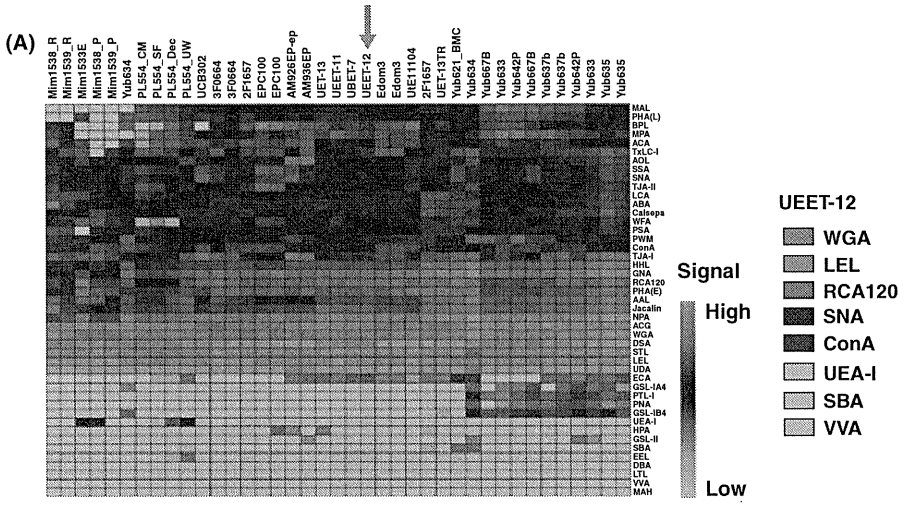

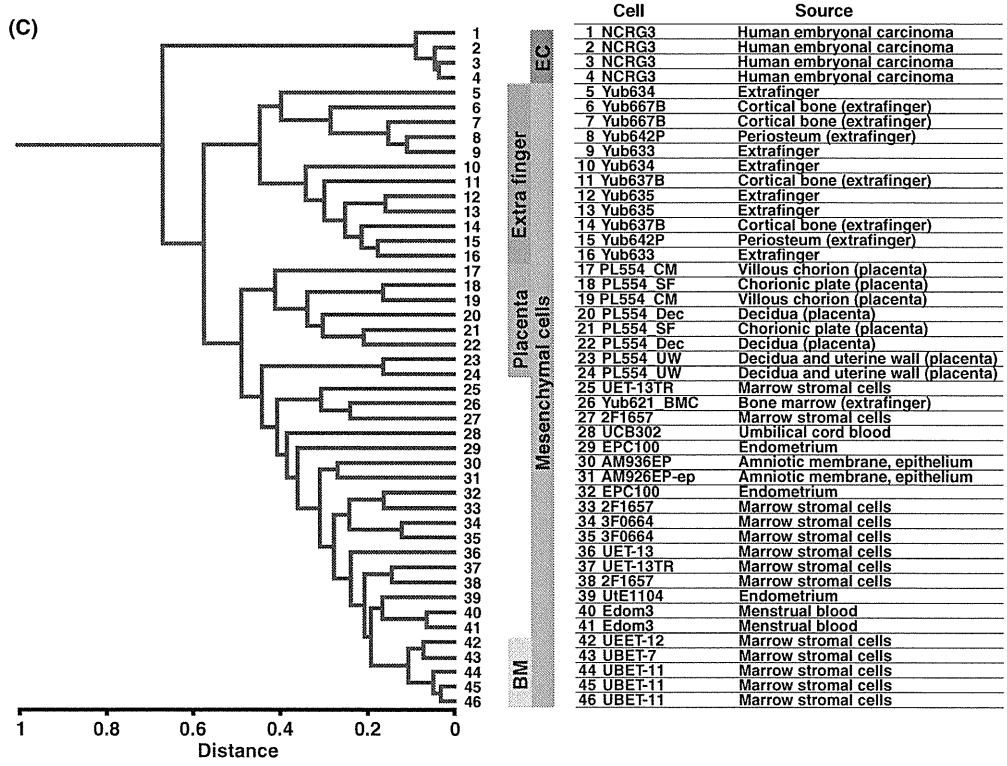

Cell	Source
1 NCRG3	Human embryonal carcinoma
2 NCRG3	Human embryonal carcinoma
3 NCRG3	Human embryonal carcinoma
4 NCRG3	Human embryonal carcinoma
5 Yub634	Extrafinger
6 Yub667B	Cortical bone (extrafinger)
7 Yub667B	Cortical bone (extrafinger)
8 Yub642P	Periosteum (extrafinger)
9 Yub633	Extrafinger
10 Yub634	Extrafinger
11 Yub637B	Cortical bone (extrafinger)
12 Yub635	Extrafinger
13 Yub635	Extrafinger
14 Yub637B	Cortical bone (extrafinger)
15 Yub642P	Periosteum (extrafinger)
16 Yub633	Extrafinger
17 PL554_CM	Villous chorion (placenta)
18 PL554_SF	Chorionic plate (placenta)
19 PL554_CM	Villous chorion (placenta)
20 PL554_Dec	Decidua (placenta)
21 PL554_SF	Chorionic plate (placenta)
22 PL554_Dec	Decidua (placenta)
23 PL554_UW	Decidua and uterine wall (placenta)
24 PL554_UW	Decidua and uterine wall (placenta)
25 UET-13TR	Marrow stromal cells
26 Yub621_BMC	Bone marrow (extrafinger)
27 2F1657	Marrow stromal cells
28 UCB302	Umbilical cord blood
29 EPC100	Endometrium
30 AM936EP	Amniotic membrane, epithelium
31 AM926EP-ep	Amniotic membrane, epithelium
32 EPC100	Endometrium
33 2F1657	Marrow stromal cells
34 3F0664	Marrow stromal cells
35 3F0664	Marrow stromal cells
36 UET-13	Marrow stromal cells
37 UET-13TR	Marrow stromal cells
38 2F1657	Marrow stromal cells
39 UtE1104	Endometrium
40 Edom3	Menstrual blood
41 Edom3	Menstrual blood
42 UEET-12	Marrow stromal cells
43 UBET-7	Marrow stromal cells
44 UBET-11	Marrow stromal cells
45 UBET-11	Marrow stromal cells
46 UBET-11	Marrow stromal cells

Figure 2 Lectin microarray analysis of human mesenchymal cells. (A) Heat map on human cells derived from extra finger (auricular cartilage), bone marrow, umbilical cord blood, amnion, menstrual blood and endometrium. (B) Flow cytometric analysis of UEET-12 marrow stromal cells using each lectin probe. Nonshaded and shaded areas indicate reactivity of antibodies for isotype controls and that of antibodies for cell surface markers, respectively. (C) Hierarchical clustering analysis was performed based on the results of lectin microarrays. Human embryonic carcinoma cells (NCR-G3) and mesenchymal cells are discriminated by color bars (EC: red, mesenchymal cells: green, bone marrow (BM): yellow, placenta: orange, extra finger: blue).

Siaα2-6Gal/GalNAc; (iii) *Narcissus pseudonarcissus* agglutinin (NPA), ConA, *Galanthus nivalis* agglutinin (GNA) and *Hippeastrum hybrid* lectin (HHL), that bind to high-mannose structures; (iv) *Datura stramonium* agglutinin (DSA), LEL, *Solanum tuberosum* lectin (STL), *Urtica dioica* agglutinin (UDA), Pokeweed mitogen (PWM) and WGA that bind to GlcNAcβ1-4GlcNAc. Osteoblasts specifically reacted to *Griffonia simplicifolia* lectin I, isolectin (GSL I) A4 and its isolectin B4 that bind to α-GalNAc and α-Gal, respectively, Peanut agglutinin (PNA) that binds to Galβ1-3GalNAc and *Psophocarpus tetragonolobus* lectin I (PTL I) that binds to α-GalNAc (Fig. S1 in Supporting Information). These results suggested the lectin microarrays are a practical tool for glycan-based category of human mesenchymal cells, and that each cell type in the various cell lineages have specific carbohydrate structures.

Lectin microarray analysis of hES cells

To study glycans during differentiation of hES cells, we performed lectin microarray analysis with extracts from undifferentiated hES cells (hES-3, 8, 9 provided from Harvard University) and differentiated hES cells after embryoid body formation (EB) (Fig. S2 in supporting Information). The lectin microarray data after statistical analysis show that undifferentiated hES cells and differentiated cells (EB) were clearly categorized (Fig. 3A). To select lectins to discriminate between ES (pluripotent) and EB (nonpluripotent) cells, we analyzed lectin signals using 'pair-wise comparison means' based on FDR (False Discovery Rate) statistics. Three lectins [MAL, PHA(L) and EEL that bind to Siaα2-3Galβ1-4GlcNAc, tri/tetra-antennary complex-type N-glycan and Galα1-3Gal, respectively] could discriminate between the individual cell populations (FDR <0.05, fold-change >2.0) (Fig. 3B). The signals of MAL and PHA(L) in hES population were lower than those in EB, whereas the EEL signal in ES was higher than that in EB (Fig. 3C, D).

Lectin microarray analysis of iPS cells

We generated human iPS cell lines from MRC-5 embryonic lung fibroblasts (Makino *et al.* 2009) (Table S4 in Supporting Information) and performed

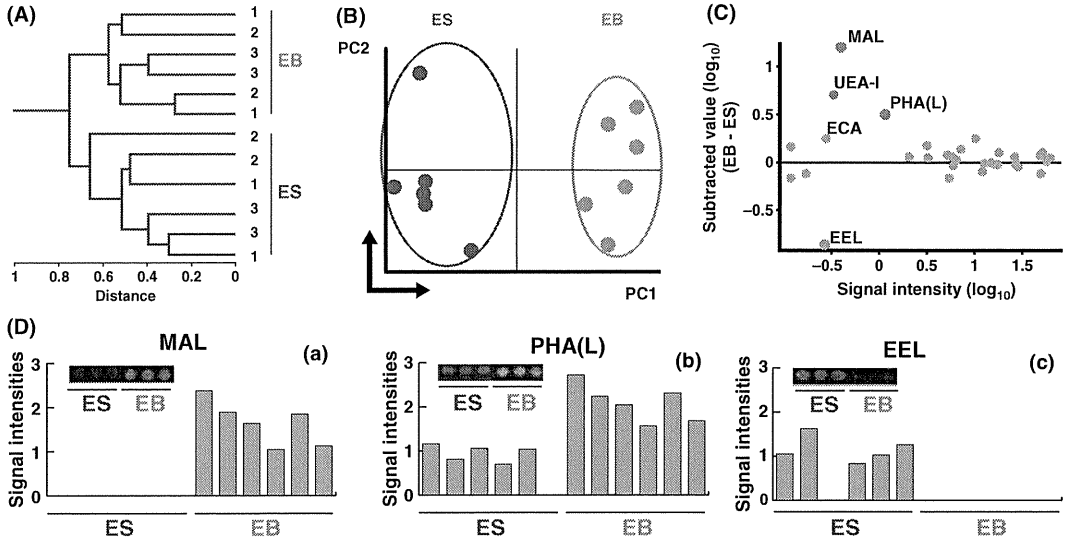

Figure 3 Lectin microarray analysis of human embryonic stem cells. (A) Hierarchical Clustering analysis of undifferentiated and differentiated ES cells. (B) Principal component analysis of lectin microarray analysis on undifferentiated and differentiated ES cells. (C) Signal value for *Maackia amurensis* lectin (MAL) processed by a max-normalization procedure after a gain-merging process. (D) Images of signal spots and signal intensities for MAL (a), PHA(L) (b), and *Euonymus europaeus* lectin (EEL) (c).

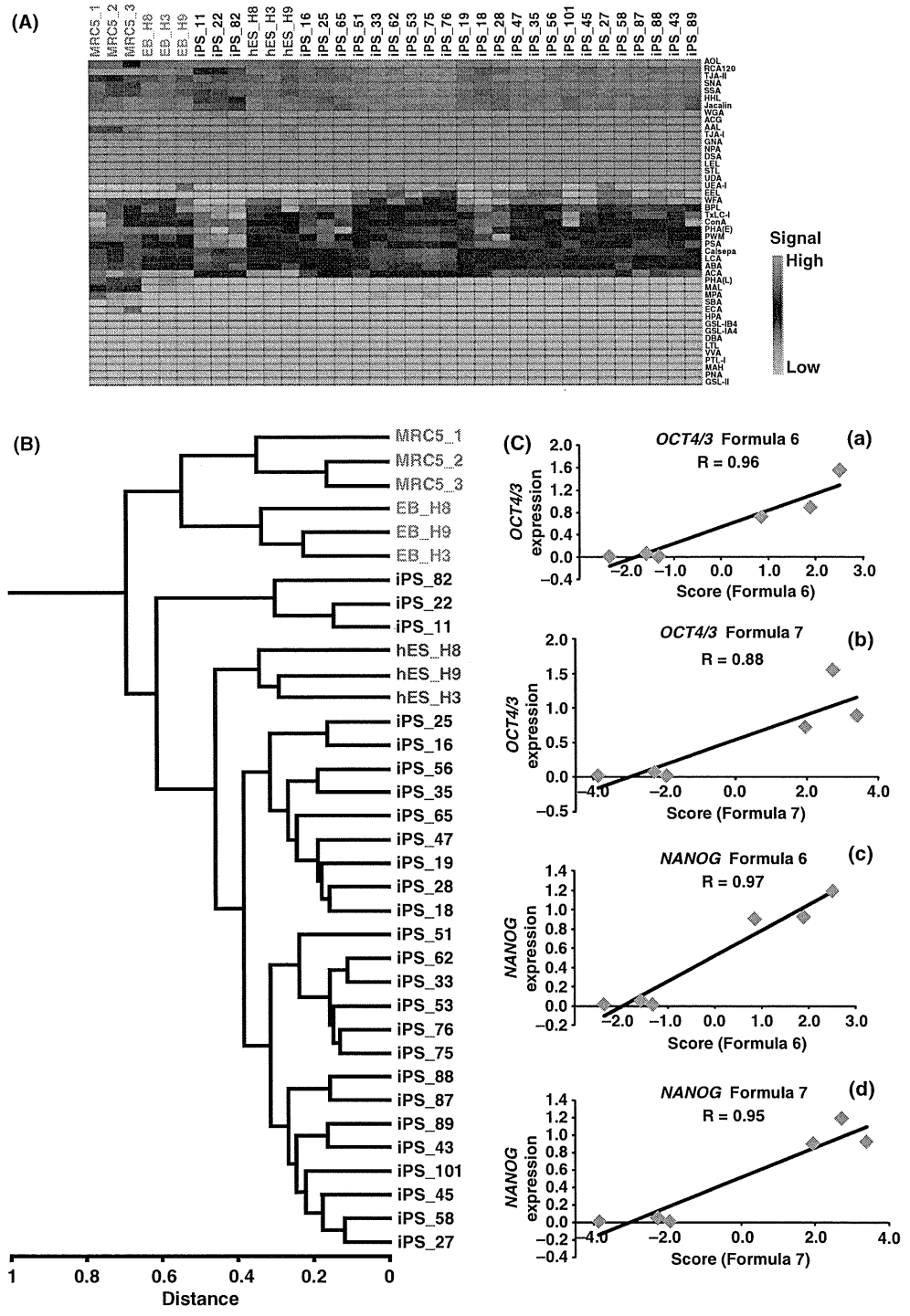

Figure 4 Lectin microarray analysis of human-induced pluripotent stem (iPS) cells. (A) Heat map of lectin microarray with MRC-5 and MRC-5-derived iPS cells. MRC-5 and iPS cells are discriminated by letter color: red, MRC-5; blue, hES cells; green, embryoid body (EB) cells; black, iPS cells. (B) Hierarchical Clustering analysis of MRC-5 and MRC-derived iPS cells. MRC-5 and iPS cells are discriminated by letter color: red, MRC-5; blue, hES cells; green, EB cells; black, iPS cells. (C) The correlation between expression of *OCT4/3* or *NANOG* and scores calculated from each formula. The correlation factors (R) are shown in each panel.